nature

https://doi.org/10.1038/s41586-022-05605-0

Accelerated Article Preview

Dendritic cells direct circadian anti-tumor immune responses

Received: 14 April 2022

Accepted: 25 November 2022

Accelerated Article Preview

Cite this article as: Wang, C. et al. Dendritic cells direct circadian anti-tumor immune responses. *Nature* https://doi.org/10.1038/s41586-022-05605-0 (2022)

Chen Wang, Coline Barnoud, Mara Cenerenti, Mengzhu Sun, Irene Caffa, Burak Kizil, Ruben Bill, Yuanlong Liu, Robert Pick, Laure Garnier, Olga A. Gkountidi, Louise M. Ince, Stephan Holtkamp, Nadine Fournier, Olivier Michielin, Daniel E. Speiser, Stéphanie Hugues, Alessio Nencioni, Mikaël J. Pittet, Camilla Jandus & Christoph Scheiermann

Dendritic cells direct circadian anti-tumor immune responses

Chen Wang[1], Coline Barnoud[1], Mara Cenerenti[1,2], Mengzhu Sun[1], Irene Caffa[3], Burak Kizil[1], Ruben Bill[1,4,5], Yuanlong Liu[6,7,8], Robert Pick[1], Laure Garnier[1], Olga A Gkountidi[1], Louise M. Ince[1], Stephan Holtkamp[9], Nadine Fournier[8], Olivier Michielin[4], Daniel E. Speiser[10], Stéphanie Hugues[1,11], Alessio Nencioni[3,12], Mikaël J. Pittet[1,2,4,5], Camilla Jandus[1,2,11], Christoph Scheiermann[1,9,11]*

[1]*Department of Pathology and Immunology, Faculty of Medicine, University of Geneva, Geneva, Switzerland*

[2]*Ludwig Institute for Cancer Research, Lausanne, Switzerland*

[3]*Department of Internal Medicine and Medical Specialties, University of Genoa, Genoa, Italy.*

[4]*AGORA Cancer Research Center, Lausanne, Switzerland*

[5]*Center for Systems Biology, Massachusetts General Hospital and Harvard Medical School, Boston, USA*

[6]*Department of Computational Biology, University of Lausanne, Lausanne, Switzerland*

[7]*Swiss Cancer Center Leman, Lausanne, Switzerland*

[8]*Translational Data Science (TDS), Swiss Institute of Bioinformatics (SIB), Lausanne, Switzerland*

[9]*Biomedical Center (BMC), Institute for Cardiovascular Physiology and Pathophysiology, Walter Brendel- Center for Experimental Medicine (WBex), Faculty of Medicine, Ludwig-Maximilians-Universität Munich, Planegg-Martinsried, Germany*

[10]*Department of Oncology, University of Lausanne, Lausanne, Switzerland*

[11]*Geneva Centre for Inflammation Research, Geneva, Switzerland*

[12]*IRCCS Ospedale Policlinico San Martino, Genoa, Italy*

* Corresponding author: Christoph.scheiermann@unige.ch

Department of Pathology and Immunology (PATIM)

Centre Médical Universitaire (CMU), University of Geneva

Rue Michel-Servet 1, 1206 Geneva, Switzerland

Tel: +41 2237 95747

Abstract

The process of cancer immunosurveillance is a mechanism of tumor suppression that can protect the host from cancer development throughout its lifetime[1,2]. Yet, it is unknown whether its effectiveness fluctuates over a single day. Here, we demonstrate that the initial time-of-day of tumor engraftment dictates ensuing tumor size across murine cancer models. Using immunodeficient mice and animals lacking lineage-specific circadian functions, we show that dendritic cells (DCs) and $CD8^+$ T cells exert circadian anti-tumor functions that control melanoma volume. Specifically, we find that rhythmic trafficking of DCs to the tumor draining lymph node (dLN) governs a circadian response of tumor antigen-specific $CD8^+$ T cells, which is dependent on circadian expression of the co-stimulatory molecule CD80. Consequently, cancer immunotherapy is more effective when synchronized with DC functions, shows circadian outcomes in mice and suggests similar effects in humans. These data demonstrate that circadian rhythms of anti-tumor immune components are not only critical for the control of tumor size but can also be exploited therapeutically.

Main text

The immune system provides sophisticated defense mechanisms that most often eliminate or contain the appearance of tumor cells in healthy tissue, and prevent the development of life-threatening cancers[1,2]. Both the innate and adaptive arms of immunity show circadian (~24h) rhythmicity in their response[3-10], so that even weeks after an initial stimulus is encountered, time-of-day immune effects are still observed[11-16] . There is evidence that cancer cells can exhibit a perturbation in their circadian clock components, which drives cancer development[17]. However, the impact of a rhythmic immune system on tumor surveillance, and the effectiveness of treatments involving the immune system, remain unknown. Here, we provide evidence that a circadian anti-tumor immune response controls tumor volume and the response to therapy.

Results

Timed engraftment dictates tumor size

To explore whether tumor volume depends on the time-of-day of tumor cell engraftment, we injected B16-F10 melanoma cells expressing ovalbumin (B16-F10-OVA) subcutaneously (s.c.) into cohorts of mice at six different times of the day ((that is, at *Zeitgeber time* 1 (ZT1; 1 h after light onset in a 12h light / 12h dark environment; 'morning'), ZT5 ('midday'), ZT9 ('afternoon'), ZT13 ('evening'), ZT17 ('midnight') and ZT21 ('early morning')) and quantified tumor size over the ensuing two weeks. To control these data, animals were housed in distinct environmental light cabinets, 12h phase-shifted to each other, allowing the simultaneous injection of the same batch of tumor cells into differently-timed recipients. Tumor size was strongly affected by the time-of-day of engraftment, yielding significantly larger tumors when inoculated in the late night (ZT21), and smaller tumors when inoculated in the late afternoon (ZT9-ZT13)

(Fig. 1a-b, Extended Data Fig. 1a). We observed similar results in two orthotopic mammary carcinoma models (E0771 and 4T1) **(Extended Data Fig. 1b-d)** and a murine colon carcinoma model (MC-38) (**Extended Data Fig. 1e).** This indicated that the time-of-day effect of engraftment on tumor size represented a phenomenon relevant across different tumor types and sites of engraftment. We further confirmed these data by quantitative imaging approaches with luciferase-expressing melanoma cells (B16-F10-OVA-Luc) **(Extended Data Fig. 1f)**. Using B16-F10 melanoma cell lines that did or did not express OVA yielded very similar results (**Extended Data Fig. 1g)**. This indicated that the observed time-of-day effect of inoculation represented a general phenotype not affected by potentially different immunogenicity of the tumor.

Circadian rhythms are defined by their persistence in the absence of environmental entraining cues, such as rhythmic light onset and offset. Transferring animals to complete darkness conditions did not alter the observed time-of-day differences, demonstrating the effect to be *bona fide* circadian in nature (**Fig.1c**). However, switching mice to a 12h inverted dark-light cycle inversed tumor size, demonstrating that the effect was not dependent on light *per se* but that it could be entrained by light, an additional feature of circadian rhythms (**Fig. 1d and Extended Data Fig. 1h**). Subjecting mice to a jet-lag protocol (**Extended Data Fig. 1h**) abrogated time-of-day differences and increased tumors, indicating that acutely altering lighting regimes negatively affected disease outcome (**Fig. 1d**). Together, these data provide unexpected evidence that tumor size is highly governed by the initial time-of-day of engraftment, driven by circadian rhythms in the host, which are entrained by light.

123 ***Circadian anti-tumor immune effects***

124 To assess whether these effects were dependent on the immune system, we injected
125 B16-F10-OVA melanoma cells during the day (ZT9) or at night (ZT21) into NSG mice,
126 which lack both adaptive and innate immune cells. Of importance, the previously
127 observed dependency of tumor volume on time-of-day engraftment was abrogated in
128 these mice, indicating the differences to be mediated by the immune system (**Fig. 1e**).
129 To define which arm of immunity was involved, we utilized *Rag2*$^{-/-}$ mice, which lack
130 an adaptive immune system. Similar to NSG mice, time-of-day differences in tumor
131 size were ablated in these animals, demonstrating the adaptive immune system to be
132 critical in mediating the phenotype (**Fig. 1e**).
133
134 We subsequently used flow cytometry to assess the immune cell infiltrates in
135 tumors 14 days after inoculation. Tumors were harvested at ZT1, in order to limit
136 variables to just the time of engraftment. Numbers of CD8$^+$ T cells were dependent on
137 the time of engraftment, with cellularity peaking when tumor inoculation occurred
138 during the day (ZT9) and troughing at night (ZT21) (**Fig. 1f and Extended Data Fig.**
139 **2a**). In contrast, the numbers of other leukocyte subsets were not affected (**Extended**
140 **Data Fig. 2b**). To assess the functional relevance of rhythmicity in the tumor immune
141 cell infiltrate, we used different antibodies to deplete specific subpopulations of
142 leukocytes. Antibody-mediated depletion of CD8$^+$ T cells or CD4$^+$ T cells – but not of
143 neutrophils – abrogated the time-of-day difference in tumor size **(Fig. 1g and Extended**
144 **Data Fig. 2c-j)**. However, only depletion of CD8$^+$ T cells increased tumor volume (**Fig.**
145 **1g**), while depletion of CD4$^+$ T cells reduced it **(Extended Data Fig. 2c**). These results
146 indicate CD8$^+$ T cells to exert anti-tumorigenic effects in a time-of-day dependent
147 manner.

148

149 ***Rhythmic anti-tumor response in DCs***

150 To explore the mechanisms controlling the time-of-day-dependent impact of
151 $CD8^+$ T cells on tumor size, we focused on the early events that potentially accounted
152 for the observed effects. Using flow cytometry and quantitative imaging approaches to
153 characterize the site of engraftment 4 hours after tumor inoculation, we found
154 $CD11c^+MHCII^+$ cells to represent the predominant leukocyte subset, with higher
155 numbers of these cells when tumor cells were inoculated at ZT9 compared to ZT21 **(Fig**
156 **2a-c** and **Extended Data Fig. 3a-c)**. Furthermore, 24h after tumor inoculation, we
157 detected more leukocytes in draining lymph nodes (dLN) of mice in which tumor cells
158 were inoculated at ZT9 compared to ZT21 **(Extended Data Fig. 3d-e)**. Specifically,
159 we observed more $CD4^+$ and $CD8^+$ T cells, including increased numbers of activated
160 central memory ($CD44^+$ $CD62L^+$) and naïve ($CD44^-$ $CD62L^+$) T cells, following ZT9
161 tumor cell engraftment **(Extended Data Fig. 3e-f)**. These dLNs also contained more
162 $CD11c^+$ cells, including $CD11b^+$ $CD11c^+$ $MHCII^{hi}$, $CD103^+$ $CD11c^+$ $MHCII^{hi}$, $CD11b^+$
163 $CD11c^+$ $MHCII^{lo}$, and $CD8^+$ $CD11c^+$ $MHCII^{lo}$ subsets **(Extended Data Fig. 3g-i)**. This
164 phenotype was also observed in the orthotopic mammary carcinoma as well as the colon
165 carcinoma models (**Extended Data Fig. 4a-g**). Under sham conditions, time-of-day
166 changes in the number of these cell types were observed but showed smaller differences
167 (**Extended Data Fig. 5a**). To further identify relevant tumor-derived antigen-
168 presenting cells (APCs) in the dLN, we used an antibody specific for SIINFEKL
169 peptide bound to $H\text{-}2K^b$ (**Extended Data Fig. 3h-i**). We found that APCs presenting
170 this antigen predominantly displayed a $CD103^+CD11c^+MHCII^{hi}$ phenotype. These
171 $CD103^+CD11c^+MHCII^{hi}$ $(SIINFEKL{:}H\text{-}2K^b)^+$ cells were also more numerous in dLNs
172 of mice inoculated with tumor cells at ZT9 **(Fig. 2d and Extended Data Fig. 3h-i)**.

This phenotype was also observed in the orthotopic E0771-OVA breast cancer model (**Extended Data Fig. 4c-d**). No differences were observed in the processing of OVA-antigen in $CD11c^+$ cells (**Extended Data Fig. 5b**), suggesting that changes in levels of antigen presentation were not responsible for the phenotype.

Using dextramer staining to detect endogenous T cells specific for H-$2K^b$/SIINFEKL in the dLN 72h after tumor engraftment, we detected higher numbers and proportions of antigen-specific $CD44^+$ $CD8^+$ T cells, when tumor inoculation was performed at ZT9 compared to ZT21 in both the melanoma and mammary carcinoma models **(Fig. 2e and Extended Data Fig. 4e)**. We also observed significantly more EdU^+ $CD8^+$ T cells and EdU^+ $CD4^+$ T cells in the dLN 48h after tumor inoculation at ZT9 compared to ZT21, demonstrating a higher T cell proliferation rate following ZT9 tumor inoculation **(Fig. 2f and Extended Data Fig. 5c)**. In an analogous manner, we performed dextramer staining to detect endogenous T cells specific for a peptide of the neoantigen Adpgk (H-$2D^b$/ASMTNMELM), expressed by MC-38 colon carcinoma cells. We detected higher numbers of $Adpgk^+$-neoantigen specific CD8 T cells in this tumor model in the dLN 72h after tumor engraftment when tumor inoculation was performed at ZT9 compared to ZT21 (**Extended Data Fig. 4f-g**). These data indicate a time-of-day-dependent generation of tumor antigen-specific $CD8^+$ T cells in the dLN to OVA-antigen as well as neoantigen and similar mechanisms at play in a subcutaneous and orthotopic engraftment setting.

Contribution of DC and T cell clocks

To investigate whether differences were driven by immune cell intrinsic mechanisms, we used *Cd4cre:Bmal1^{flox}* mice, where the key circadian clock gene

198 *Bmal1 (*encoded by *Arntl)* is specifically deleted in T cells (*Bmal1*$^{\Delta Tcell}$), rendering them
199 arrhythmic. *Bmal1*$^{\Delta Tcell}$ mice showed similar kinetics of tumor volume when tumor cells
200 were inoculated either at ZT9 or ZT21, demonstrating the importance of T cell-intrinsic
201 rhythms in the control of tumor size **(Fig. 2g)**. Similarly, *Clec9acre:Bmal1*^{flox} mice,
202 which lack BMAL1 expression in conventional DCs (*Bmal1*$^{\Delta cDC}$), showed comparable
203 tumor size kinetics when tumor cells were inoculated either at ZT9 or ZT21 **(Fig. 2h)**.
204 This demonstrated BMAL1 and cell-autonomous circadian oscillations in both DCs and
205 T cells to be critical for the time-of-day differences in tumor volume. Mechanistically,
206 *Bmal1* deletion in cDCs abrogated differences in total and antigen-specific DC numbers
207 in the dLN after tumor engraftment, in contrast to control animals **(Fig. 2i)**. Furthermore,
208 dextramer staining in *Bmal1*$^{\Delta cDC}$ mice revealed reduced antigen-specific CD8^{+} T cell
209 levels and abrogated time-of-day differences (**Fig. 2j**). These data demonstrate DC and
210 T cell autonomous circadian clocks to be responsible for the time-of-day-dependent
211 anti-tumor effects, with DCs governing rhythmic CD8^{+} T cell responses.
212
213 ***DCs govern rhythmic anti-tumor immunity***
214 To obtain global information on DC changes after tumor inoculation at different
215 times of the day, we performed RNA sequencing (RNAseq) analyses of the subset of
216 CD11c^{+} MHCII^{hi} migratory DCs in the dLN collected 24 hours after tumor engraftment
217 or sham conditions, inoculated at ZT3, 9, 15 or 21. We observed strong time-of-day
218 differences in overall gene expression, indicating differences in DC functionality. First,
219 we found that CD11c^{+} MHCII^{hi} cells exhibited rhythmicity in the expression of clock
220 genes and clock-controlled genes (**Extended Data Fig. 6a**), with the expression of
221 these genes being sufficient to define the time of day from which the cells were derived
222 (**Extended Data Fig. 6b**). Next, we detected two main clusters of oscillatory genes,

one of which was expressed more highly in the morning (ZT9) and the other in the evening (ZT15) (**Fig. 3a-b**). Whereas the morning cluster consisted mainly of metabolic genes – with the exception of the co-stimulatory molecule CD80 – the second cluster was highly enriched in T cell activation pathways (**Fig. 3b-d, Fig. 4a and Extended Data Fig. 6c-d**). In contrast, RNAseq analyes of $CD11c^{+}$ $MHCII^{hi}$ cells harvested from *Bmal1*$^{\Delta cDC}$ mice showed altered rhythmicity, gene expression patterns and cellular pathways compared to controls (**Fig. 3b, d, Fig. 4a, Extended Data Fig. 6c and Extended Data Fig. 7a-c**). These data indicated that, in addition to differences in DC numbers, the rhythmicity in DC co-stimulatory factors that was specific for the tumor scenario (**Extended Data Fig. 8a-c)** could be responsible for the generation of rhythmic $CD8^{+}$ T cell activation phenotypes.

CD80 expression was confirmed to be time-of-day-dependent in different $CD11c^{+}$ subsets at the protein level by flow cytometry (**Fig. 4b**). To interrogate whether oscillations in CD80 were driven by a cell-autonomous circadian rhythm – independent of the environment as indicated by the RNAseq data (**Fig. 4a**) – we performed *in vitro* synchronization assays of immature as well as LPS-matured bone marrow-derived DC (BMDCs) using a serum shock[18,19] **(Fig. 4c and Extended Data Fig. 9a-c)**. We detected significant differences in *Cd80* expression at different time points after BMDC synchronization **(Fig. 4c and Extended Data Fig. 9c)**. In contrast, we observed no circadian differences in the expression of various cytokines but rather a timer-dependent progressive change through time (**Extended Data Fig. 9d)**. Furthermore, circadian differences in *Cd80* expression were abrogated in $CD11c^{+}$ $MHCII^{hi}$ cells harvested from *Bmal1*$^{\Delta cDC}$ *in vivo* as well as BMDCs generated from mice lacking overall expression of circadian genes *in vitro* (*Bmal1*$^{-/-}$ or *Per1*$^{-/-}$*Per2*$^{-/-}$) (**Fig. 4a, c-d**). To further test whether circadian rhythmicity in myeloid cells was necessary to control

Cd80 expression, we assessed BMDCs produced from mice lacking BMAL1 specifically in myeloid cells (*Lyz2cre:Bmal1*^{flox}*; Bmal1*$^{\Delta myeloid}$); again, we found that loss of BMAL1 abrogated time-of-day differences in CD80 expression (**Fig. 4e**). Taken together, these findings indicate a critical role for the circadian clock machinery in controlling CD80 expression.

To investigate whether the circadian rhythmicity in DC gene expression patterns had a functional and causal consequence on T cell activation, we performed co-culture experiments of synchronized, SIINFEKL-pulsed BMDCs with non-synchronized OVA-specific OT-I CD8$^+$ T cells. This approach allowed us to observe that the rhythmicity of DCs directly controlled that of T cells. Indeed, the proliferation of OT-I CD8$^+$ T cells was highly dependent on the rhythmic phase in which the DCs were located (**Fig. 4f**). BMDCs harvested 36h after synchronization induced stronger OT-I T cell proliferation than BMDCs harvested 24h after synchronization **(Fig. 4f)**. In contrast, BMAL1-deficient BMDCs failed to induce rhythmic OT-I CD8$^+$ T cell proliferation (**Fig. 4g**). Furthermore, treatment with an anti-CD80 antibody abrogated time-of-day differences in OT-I CD8$^+$ T cell proliferation (**Fig. 4h**), demonstrating the relevance of CD80 in the rhythmic CD8$^+$ T cell response.

To specifically investigate the importance of rhythmicity in co-stimulatory signals provided by BMDCs, we performed co-culture experiments of synchronized, SIINFEKL-pulsed BMDCs with non-synchronized OVA-specific OT-I CD8$^+$ T cells, as before, but bypassing MHCI-TCR interactions using an anti-CD3 antibody. Co-stimulatory signals, in the presence of isotype-matched control antibodies, were sufficient to promote time-of-day differences in OT-I CD8$^+$ T cell proliferation;

however, anti-CD80 treatment abrogated these time-of-day differences (**Fig. 4i**). Finally, antibody treatment against CD80 abrogated the differences in tumor volume after time-of-day dependent engraftment (**Fig. 4j**), demonstrating the functional relevance of CD80 *in vivo* in driving differences in tumor size. These data indicate that CD80 is a critical molecule in this process.

In addition, we identified the presence of BMAL1-binding sites, namely canonical enhancer boxes (E-boxes), in the promoter region of the *Cd80* gene. This suggests that *Cd80* expression is directly regulated by the circadian clock (**Extended Data Fig. 9e**). Indeed, using ChIP assays, we confirmed rhythmic binding of BMAL1 to the *Cd80* promoter (**Fig. 4k and Extended Data Fig. 9f**). Together, these data demonstrate that circadian rhythms in DCs direct the rhythms of T cell proliferation, a phenomenon dependent on the rhythmic expression of CD80, which is under direct transcriptional control of the clock gene BMAL1.

Vaccination tumor chrono-immunotherapy

To evaluate the translational potential of our findings, we explored tumor chrono-immunotherapy. Specifically, we studied mice inoculated with B16-F10-OVA melanoma cells at ZT9 and then immunized with OVA either during the day (ZT9) or at night (ZT21). This setting limited the time-of-day information to the timepoint of vaccination only. Strikingly, we found that tumor volume was strongly suppressed by the vaccine when administered to wild-type mice at ZT9 compared to ZT21 **(Fig. 5a)**, even when the relative incubation time of the vaccine was significantly longer for ZT21 than for ZT9 (**Extended Data Fig. 10a)**. In contrast, *Bmal1*$^{\Delta cDC}$ mice vaccinated with OVA at ZT9 or ZT21 showed similar tumor sizes (**Fig. 5b**). Analysis of dLNs from

wild-type mice 24h after vaccination revealed a higher number of SIINFEKL-presenting DCs in mice vaccinated at ZT9 compared to those vaccinated at ZT21 (**Figure 5c and Extended Data Fig. 10b**). Furthermore, this increase at ZT9 coincided with higher numbers of $CD69^+$ $CD8^+$ and $CD69^+$ $CD4^+$ T cells **(Fig. 5d and Extended Data Fig. 10c)**. In contrast, DC and T cell numbers and phenotypes remained similar in *Bmal1*$^{\Delta cDC}$ mice vaccinated at ZT9 or ZT21 **(Fig. 5c-d and Extended Data Fig. 10b-c)**. These data indicate a key role of cDC rhythmicity in generating a productive anti-tumor immune response following treatment.

We further performed vaccination experiments at ZT9 and ZT21 in a scenario which also tumors where inoculated at ZT9 and ZT21, thus assessing the contribution of time-of-day effects in both the timing of tumor inoculation and the timing of vaccination. In these experiments, we observed that the timing of vaccination had a greater impact than the timing of tumor inoculation on tumor burden (**Extended Data Fig. 10d**). Also, we confirmed the time-of-day differences in vaccine efficacy in additional experiments in which two vaccinations were performed at ZT9 or ZT21 several days apart (**Extended Data Fig. 10e).** These data demonstrate that the timing of vaccination is a powerful means of reducing tumor size, and that rhythmicity of cDCs plays a critical role in this process.

To bypass any endogenous DCs acting as potential APCs in this scenario, we performed vaccinations with s.c. injections of SIINFEKL peptide-loaded BMDCs during the day (ZT9) or at night (ZT21). These experiments showed very similar results to the antigen vaccination studies, with suppressed tumor volume after daytime administration of the BMDCs (**Fig. 5e**). To assess whether these observations could

translate to humans, we generated human monocyte-derived DCs (hMoDCs) from $CD14^+$ primary monocytes isolated from buffy coats from healthy donors and synchronized them *in vitro*. hMoDCs exhibited a circadian expression of *CD80* as well as of the clock gene *PER2* (**Fig. 5f-g and Extended Data Fig. 10f**), analogous to the results obtained in mice. Furthermore, co-culture experiments using synchronized hMoDCs together with naïve $CD8^+$ T cells isolated from the same healthy donors and stimulated with anti-human CD3 antibody – thus limiting rhythmicity to co-stimulatory factors in DCs only – showed an increased T cell proliferation in hMoDC 36h after synchronization compared to the 24h time point (**Fig. 5h**).

Moreover, by generating HLA-$A2^+$ MoDCs, pulsed with Melan-$A_{26\text{-}35(A27L)}$ peptide (ELAGIGILTV; 'ELA') and co-cultured with HLA-A2/ELA-specific $CD8^+$ T cell clones derived from malignant melanoma patients[20], we observed time-of-day differences in the T cell proliferation capacity (**Fig. 5i**). This indicated that the rhythmic anti-tumor responses we observed in mice were also present in human cells. Indeed, using retrospective time-of-day analyses of a tumor vaccination trial including 10 HLA-$A2^+$ patients with advanced malignant melanoma[20], we observed time-of-day differences in vaccine administration to result in increased Melan-A-specific $CD8^+$ T cells in patients' blood, when vaccinations were perfomed in the morning compared to the afternoon (**Fig. 5j**). Together, these data provide evidence for an unexpected role of time-of-day in tumor engraftment and in the efficacy of cancer immunotherapy in mice and humans.

In this study, we focused mostly on a mouse model of melanoma, while our additional data indicate that other cancer types are also affected by a rhythmic immune system; however, whether similar immune mechanisms are at play in other tumor

models remains to be formally demonstrated. Furthermore, our initial patient data indicate the importance of considering the time of day for the administration of cancer immunotherapy. By extension, it is possible that the time of day for the administration of any other treatment that involves activation of the immune system may matter. Given the relative simplicity of controlling this timing parameter in the clinic, it seems important to conduct prospective clinical trials that include sufficient numbers of patients and that can test whether the timing of injection of a given treatment improves the anti-tumor response and the patient's clinical outcome.

Figure Legends

Figure 1. Time-of-day of engraftment dictates tumor size

(a) Tumor volume after engraftment of B16-F10-OVA cells at 6 different times of the day (*Zeitgeber* time (ZT)); n=10 mice from 2 independent experiments, two-way ANOVA. **(b)** Tumor volume on day 14 from **a**, Cosinor analysis. **(c)** Tumor volume after engraftment of B16-F10-OVA cells at 2 different times of the day under constant darkness (DD) conditions (circadian time (CT)); n=6 mice, from 2 independent experiments, two-way ANOVA. **(d)** Tumor volume after engraftment of B16-F10-OVA at 2 different times of the day under light:dark (LD, n=6 mice), inverted dark:light (DL, n=7 mice), or jet lag (JL, n=7 mice) conditions, from 2 independent experiments, two-way ANOVA. **(e)** Tumor volume after engraftment of B16-F10-OVA at 2 different times of the day in NSG mice (left, n=10 mice) or *Rag2*$^{-/-}$ mice (right, n=10 (ZT9), and n=11 (ZT21) mice). Control WT mice (n=9) are plotted as reference. Data are from 2 independent experiments, two-way ANOVA. **(f)** Tumor infiltrating CD8^{+} T cells on day 14 from **a**; from ZT1 to 21, n = 10, 9, 10, 7, 10, 8 mice from 4 independent experiments, Cosinor analysis. **(g)** Tumor volume after engraftment of B16-F10-OVA at 2 different times of the day after anti-CD8 antibody depletion; n=6 mice from 2 independent experiments, two-way ANOVA. Shaded areas indicate dark phases. All data are represented as mean ± SEM, ns, not significant.

Figure 2. Dendritic cells respond rhythmically to tumor engraftment

(a) Number of cells at the skin engraftment site 4h after B16-F10-OVA engraftment at 2 different times of the day, n=8 mice from 2 independent experiments, unpaired Student's *t*-test. **(b-c)** Imaging (scale bar 500µm) (**b**), and quantification (**c**) of CD11c^{+} cells of the skin engraftment site 4h after B16-F10-OVA cell engraftment; n=6 mice from 2 independent experiments, unpaired Student's *t*-test. **(d)** Numbers of cells in the dLN 24h after B16-F10-OVA cell engraftment; n=8 mice from 2 independent experiments, unpaired Student's *t*-test. **(e)** H-2K^{b}/SIINFEKL dextramer staining of CD8^{+} T cells in the dLN 72h after B16-F10-OVA engraftment; n=8 (ZT9) and n=7 (ZT21) mice from 2 independent experiments, unpaired Student's *t*-test. **(f)** EdU staining gated on CD3^{+}CD8^{+} T cells in the dLN 48h after B16-F10-OVA cell engraftment; n=3 (ZT9) and 4 (ZT21) mice, representative from 2 independent experiments, unpaired Student's *t*-test. **(g-h)** Tumor volume after engraftment of B16-F10-OVA cells in *Cd4cre:Bmal1*^{flox} mice, n=8 (ZT9 control), n=16 (ZT9 *Cre*), n=16 (ZT21 control), and n=7 (ZT21 *Cre*) (**g**), and *Clec9acre:Bmal1*^{flox} mice, n=17 (ZT9 control), n=9 (ZT9 *Cre*), n=16 (ZT21 control), and n=10 (ZT21 *Cre*) (**h**), from 3 independent experiments, two-way ANOVA. **(i)** Numbers of CD11c^{+}MHCII^{hi} subsets in the dLN 24h after B16-F10-OVA cell engraftment in *Clec9acre:Bmal1*^{flox} mice, n=8 (ZT9 control), n=7 (ZT9 *Cre*), n=7 (ZT21 control), and n=6 (ZT21 *Cre*) from 2 independent experiments, unpaired Student's *t*-test. **(j)** H-2K^{b}/SIINFEKL dextramer staining of CD8^{+} T cells in the dLN 72h after B16-F10-OVA cell engraftment in

Clec9acre:Bmal1^{flox} mice; n=8 (ZT9 control), n=7 (ZT9 *Cre*), n=7 (ZT21 control), and n=8 (ZT21 *Cre*) mice from 2 independent experiments, unpaired Student's *t*-test. All data are represented as mean ± SEM, ns, not significant, all *t*-tests are two-tailed.

Figure 3. DCs exhibit circadian gene expression patterns

(a-d) RNAseq analyses of CD11c^{+} MHCII^{hi} cells in the dLN 24h after B16-F10-OVA cell engraftment at ZT3, ZT9, ZT15 or ZT21 in control mice (n=5 mice) or *Clec9acre:Bmal1*^{flox} mice (n=3 mice), from 2 independent experiments. (**a**) Principal component (PC) analyses of the two main peaks in gene expression oscillation in control mice; n=5 mice, Cosinor analysis. **(b)** Significantly enriched GO pathways from PC2 in control cells (**a**), with T cell activation pathways highlighted in red, shown for control and *Clec9acre:Bmal1*^{flox} CD11c^{+} MHCII^{hi} cells. The vertical dashed line represents the significant *P* values, hypergeometric test. **(c)** Significantly expressed genes in the CD28 dependent PI3K/Akt signaling pathway (top) or T cell activation pathways (bottom) in control mice and **(d)** lack of significance in *Clec9acre:Bmal1*^{flox} mice.

Figure 4. Rhythmic expression of CD80 in DCs governs T cell responses

(a) Expression (counts per million (CPM)) of *Cd80* in CD11c^{+} MHCII^{hi} cells from control (n=5) or *Clec9acre:Bmal1*^{flox} mice (n=3), one-way ANOVA. **(b)** CD80 expression in DCs subsets by flow cytometry in dLN 24h after B16-F10-OVA cell engraftment; n=6 mice from 2 independent experiments, one-way ANOVA. **(c)** *Cd80* mRNA expression after synchronization of LPS-matured BMDCs from WT (n=10) and *Bmal1*$^{-/-}$ (n=4) mice from 2 independent experiments, Cosinor analysis. **(d)** *Cd80* mRNA expression after synchronization of BMDCs generated from WT (n=4) *Per1*$^{-/-}$ *Per2*$^{-/-}$ (n=2) or *Bmal1*$^{-/-}$ mice (n=4), from 2 independent experiments, unpaired Student's *t*-test. **(e)** CD80 protein expression in synchronized *Lyz2cre:Bmal1*^{flox} BMDCs by flow cytometry; n=4 (control), n=5 (*Cre*) mice from 2 independent experiments, paired Student's *t*-test. **(f-h)** *In vitro* co-culture proliferation experiments with OT-I CD8^{+} T cells and SIINFEKL loaded BMDCs generated from WT mice (n=3 mice from 2 independent experiments), one-way ANOVA **(f)**, or *Bmal1*$^{-/-}$ mice (n=4, from 2 independent experiments), unpaired Student's *t*-test **(g)** or anti-CD80 antibody treatment **(h)**, n=9 (control) and n=5 (anti-CD80) mice from 9 independent experiments, paired Student's *t*-test. **(i)** *In vitro* co-culture proliferation experiments with naïve CD8^{+} T cells, anti-CD3 antibody and WT BMDCs in the presence of absence of anti-CD80 antibody; n=3 mice 2 replicates each, from 2 independent experiments, unpaired Student's *t*-test. **(j)** Tumor volume after engraftment of B16-F10-OVA cells at 2 different times of the day and anti-CD80 or isotype control treatment, n=10 mice from 2 independent experiments, two-way ANOVA. **(k)** Chromatin immunoprecipitation (ChIP) of BMAL1 binding to the promoter region of *Cd80* in synchronized BMDCs,

n=3 mice, from 2 independent experiments, unpaired Student's *t*-test. All data are represented as mean ± SEM, ns, not significant, all *t*-tests are two-tailed.

Figure 5. Chronotherapeutic vaccination as tumor immunotherapy

(a) Tumor volume after engraftment of B16-F10-OVA cells at ZT9 and OVA vaccination on day 5 (arrow) at ZT9 or ZT21; n=12 mice, and n=3 unvaccinated control mice from 2 independent experiments, two-way ANOVA. **(b)** Tumor volume after engraftment of B16-F10-OVA cells with OVA vaccination on day 5 (arrow) at ZT9 or ZT21 in control or *Clec9acre:Bmal1*^{flox} mice; n=5 mice from 2 independent experiments, two-way ANOVA. **(c-d)** Numbers of DC subsets **(c)** and T cells **(d)** in the dLN 24h after OVA vaccination (on day 5 after B16-F10-OVA cell engraftment) in control or *Clec9acre:Bmal1*^{flox} mice, n=5 mice from 2 independent experiments, unpaired Student's *t*-test. **(e)** Tumor volume after B16-F10-OVA cell engraftment with SIINFEKL-loaded BMDC vaccination on day 5 (arrow) at ZT9 or ZT21; n=6 mice from 2 independent experiments, two-way ANOVA. **(f)** mRNA expression of *CD80* in human monocyte derived DCs (hMoDC) after synchronization; n=3 patients, Cosinor analysis. **(g)** Human CD80 protein expression by flow cytometry in hMoDC after synchronization; n=7 patients, paired Student's *t*-test. **(h)** *In vitro* co-culture proliferation experiments with human naïve $CD8^+$ T cells and synchronized-hMoDC, n=4 patients, paired Student's *t*-test. **(i)** *In vitro* co-culture proliferation experiments with antigen specific $CD8^+$ T cells from melanoma patients and synchronized $HLA\text{-}A2^+$ hMoDC, data are technical replicates, representative from 2 donors from two independent experiments, unpaired Student's *t*-test. **(j)** Fold change of Melan-A specific T cells after 2 and 4 vaccinations (with Melan-A peptide, CpG 7909 and incomplete Freund's adjuvant) in the morning (n=6) or afternoon (n=4) patients, linear regression analysis. All data are represented as mean ± SEM, ns, not significant, all *t*-tests are two-tailed.

References

1 Gajewski, T. F., Schreiber, H. & Fu, Y. X. Innate and adaptive immune cells in the tumor microenvironment. *Nat Immunol* **14**, 1014-1022, doi:10.1038/ni.2703 (2013).

2 Chen, D. S. & Mellman, I. Elements of cancer immunity and the cancer-immune set point. *Nature* **541**, 321-330, doi:10.1038/nature21349 (2017).

3 Arjona, A., Silver, A. C., Walker, W. E. & Fikrig, E. Immunity's fourth dimension: approaching the circadian-immune connection. *Trends Immunol* **33**, 607-612, doi:10.1016/j.it.2012.08.007 (2012).

4 Curtis, A. M., Bellet, M. M., Sassone-Corsi, P. & O'Neill, L. A. Circadian clock proteins and immunity. *Immunity* **40**, 178-186, doi:10.1016/j.immuni.2014.02.002 (2014).

5 Labrecque, N. & Cermakian, N. Circadian Clocks in the Immune System. *J Biol Rhythms* **30**, 277-290, doi:10.1177/0748730415577723 (2015).

6 Man, K., Loudon, A. & Chawla, A. Immunity around the clock. *Science* **354**, 999-1003, doi:10.1126/science.aah4966 (2016).

7 Pick, R., He, W., Chen, C. S. & Scheiermann, C. Time-of-Day-Dependent Trafficking and Function of Leukocyte Subsets. *Trends Immunol* **40**, 524-537, doi:10.1016/j.it.2019.03.010 (2019).

8 Scheiermann, C., Gibbs, J., Ince, L. & Loudon, A. Clocking in to immunity. *Nature reviews. Immunology* **18**, 423-437, doi:10.1038/s41577-018-0008-4 (2018).

9 Scheiermann, C., Kunisaki, Y. & Frenette, P. S. Circadian control of the immune

system. *Nature reviews. Immunology* **13**, 190-198, doi:10.1038/nri3386 (2013).

10 Palomino-Segura, M. & Hidalgo, A. Circadian immune circuits. *J Exp Med* **218**, doi:10.1084/jem.20200798 (2021).

11 Druzd, D. *et al.* Lymphocyte Circadian Clocks Control Lymph Node Trafficking and Adaptive Immune Responses. *Immunity* **46**, 120-132, doi:10.1016/j.immuni.2016.12.011 (2017).

12 Fortier, E. E. *et al.* Circadian variation of the response of T cells to antigen. *J Immunol* **187**, 6291-6300, doi:10.4049/jimmunol.1004030 (2011).

13 Silver, A. C., Arjona, A., Walker, W. E. & Fikrig, E. The circadian clock controls toll-like receptor 9-mediated innate and adaptive immunity. *Immunity* **36**, 251-261, doi:10.1016/j.immuni.2011.12.017 (2012).

14 Sutton, C. E. *et al.* Loss of the molecular clock in myeloid cells exacerbates T cell-mediated CNS autoimmune disease. *Nat Commun* **8**, 1923, doi:10.1038/s41467-017-02111-0 (2017).

15 Long, J. E. *et al.* Morning vaccination enhances antibody response over afternoon vaccination: A cluster-randomised trial. *Vaccine* **34**, 2679-2685, doi:10.1016/j.vaccine.2016.04.032 (2016).

16 de Bree, L. C. J. *et al.* Circadian rhythm influences induction of trained immunity by BCG vaccination. *J Clin Invest* **130**, 5603-5617, doi:10.1172/JCI133934 (2020).

17 Papagiannakopoulos, T. *et al.* Circadian Rhythm Disruption Promotes Lung Tumorigenesis. *Cell Metab* **24**, 324-331, doi:10.1016/j.cmet.2016.07.001

(2016).

18 Balsalobre, A., Damiola, F. & Schibler, U. A serum shock induces circadian gene expression in mammalian tissue culture cells. *Cell* **93**, 929-937, doi:10.1016/s0092-8674(00)81199-x (1998).

19 Holtkamp, S. J. *et al.* Circadian clocks guide dendritic cells into skin lymphatics. *Nat Immunol* **22**, 1375-1381, doi:10.1038/s41590-021-01040-x (2021).

20 Speiser, D. E. *et al.* Rapid and strong human CD8+ T cell responses to vaccination with peptide, IFA, and CpG oligodeoxynucleotide 7909. *J Clin Invest* **115**, 739-746, doi:10.1172/JCI23373 (2005).

Materials and Methods

Animals

C57BL/6N and NSG mice were purchased from Charles River, BALB/c mice were purchased from Envigo. *Rag2*$^{-/-}$ mice (gift from Walter Reith, University of Geneva, Switzerland) were bred at Charles River. Other transgenic mouse lines were bred at ENVIGO: *Bmal1*$^{flox/flox}$, *Cd4cre* (both purchased from Jackson Labs) and *Clec9acre* (gift from Barbara Schraml, LMU Munich, Germany). Transgenic mice were maintained as homozygous for *Bmal1*$^{flox/flox}$ and heterozygous for the relevant Cre. CD45.1 OTI (gift from Walter Reith) mice and *Bmal1*$^{-/-}$ (gift from Charna Dibner, University of Geneva, Switzerland) mice were bred in house. All mice used were females at 8-12 weeks of age. Mice were housed under a 12 h:12 h light:dark schedule with food and water *ad libitum*. When multiple time points were investigated simultaneously, light-tight cabinets (Techniplast) were used to shift animals to the respective phase for a minimum of 1 day per 1h of shift prior to the experiments. Treatment times correspond to *Zeitgeber* time (ZT) and indicate timing relative to lights on in the animal facility such that ZT1 is 1 h after lights on (morning), ZT7 is 7 h after lights on (day time), ZT13 is 1 h after lights off (evening) and ZT19 is 7 h after lights off (night time). Animals were humanely euthanized if the tumor diameter reached 1.5 cm. All animal procedures and experiments were approved and performed in accordance with the guidelines of the animal research committee of Geneva, Switzerland or by the Italian Istituto Superiore di Sanità (ISS).

552

553 **Tumor cell lines and inoculation**

554 B16-F10 (ATCC) and B16-F10-OVA melanoma cells (gift from Stéphanie Hugues,
555 University of Geneva, Switzerland) were maintained in RPMI (Gibco) supplemented
556 with 10% heat-inactivated FCS (Gibco), 100 µmol/L penicillin–streptomycin (Gibco),
557 and 50 mmol/L of β-mercaptoethanol (Gibco). B16-F10-OVA-Luc were created using
558 ready-to-use lentivirus (GenTarget, LVP324) according to the manufacturer's
559 instructions. Transduced cells were selected by puromycin (ThermoFisher, A1113803)
560 and isolated by fluorescence-activated cell sorting (FACS). MC38 murine colon
561 adenocarcinoma cells (gift from Stéphanie Hugues, University of Geneva, Switzerland)
562 were maintained in DMEM (Gibco), 10% heat-inactivated FCS, 100 µmol/L penicillin–
563 streptomycin and 50 mmol/L of β-mercaptoethanol. E0771 and E0771-OVA (gift from
564 Stéphanie Hugues, University of Geneva, Switzerland) were maintained in RPMI
565 (Gibco) supplemented with 10% heat-inactivated FCS (Gibco), 100 µmol/L penicillin–
566 streptomycin (Gibco), and 50 mmol/L of β-mercaptoethanol (Gibco). The 4T1 cell line
567 was purchased from ATCC and maintained in RPMI1640 medium supplemented with
568 10% heat-inactivated FBS, penicillin (50 units/ml), and streptomycin (50 µg/ml)
569 (LifeTechnologies, Italy). Cell lines were used by passage 10 and tested negative
570 for *Mycoplasma*. Unless otherwise specified, 5×10^5 tumor cells in 100µl PBS were
571 injected subcutaneously (s.c.) into the right flank of mice, under isoflurane anesthesia.
572 5×10^5 4T1, E0771, or E0771-OVA cells resuspended in PBS were injected
573 orthotopically into the fourth abdominal fat pad of BALB/c (4T1) or C57BL/6 (E0771,

574 E0771-OVA) female mice under ketamine/xylazine anesthesia. Tumor volume was
575 monitored every 1 to 2 days using a caliper and calculated by length × width× width/2.
576 Time-of-day of measurements did not influence tumor volume (data not shown). In a
577 sham injection experiment, 100 µl of PBS were injected subcutaneously without tumor
578 cell injection.
579
580 **IVIS imaging**
581 D-Luciferin (Abcam ab143655, 150) was injected intraperitoneally (i.p.) into mice at a
582 dose of 75 mg/kg body weight. Mice were anaesthetized with isoflurane and placed in
583 the abdominal position. Images were collected 8 min after luciferin injection using the
584 IVIS Imaging System (Xenogen, Alameda, CA), and photons emitted from the tumor
585 were quantified using Living Image Software (Xenogen).
586
587 **Bone Marrow-Derived Dendritic Cells**
588 Bone marrow-derived dendritic cells (BMDCs) were cultured as previously described[21],
589 with complete culture media (RPMI, 10% heat-inactivated FCS, 2 mM L-glutamine, 1%
590 penicillin-streptomycin, 50 µM β-mercaptoethanol) supplemented with 20 ng/ml
591 recombinant murine GM-CSF (Peprotech). The medium was refreshed every 3 days.
592 At day 10, all non- and semi-adherent cells were collected in complete media
593 supplemented with 10 ng/ml GM-CSF and stimulated with 100 ng/ml
594 lipopolysaccharide (LPS, L4516, Sigma-Aldrich) for 24 hours.
595

BMDC synchronization

Cells were synchronized as previously described [18]. In brief, an equal volume of horse serum (Sigma, h1270) was pre-warmed and added directly to the dish (serum shock). After 2h incubation at 37°C with 5% CO2, cells were washed and resuspended in complete medium.

Tissue digestion and single-cell preparation

The draining inguinal lymph node was collected and chopped into small pieces, then digested in 1 mL RPMI containing 1mg/mL collagenase IV (Worthington Biochemical Corporation), 40 µg/mL DNase I (Roche 04716728001) and 2% heat-inactivated FCS for 15 minutes at 37 °C using a thermoblock. Skin tissue was digested in RPMI containing 1mg/mL collagenase IV, 2mg/mL Dispase II (Roche), 40 µg/mL DNase I and 2% heat-inactivated FCS for 30 minutes at 37 °C. Chopped tumor tissue was digested using 1mg/mL collagenase IV, 40µg/mL DNase I and 2% heat-inactivated FBS for 30 minutes at 37 °C, and the remaining tumor went through 30 min further digestion using 1 mg/mL collagenase D (Roche). Cells were rinsed through a 70 µm cell strainer to obtain single-cell suspensions.

Flow Cytometry

Single-cell suspensions were prepared and incubated with mouse or human Fc receptor block (anti-mouse CD16/32 Biolegend, human FcR blocking reagent, Miltenyi Biotec)

for 10 minutes at room temperature (RT). After incubation, unless specified otherwise, the antibody mix was added directly into the cell suspension and incubated for 15 min at 4°C.

The following anti-mouse antibodies were used for immunostaining: CD45 (clone 30-F11, BUV 395, BUV 737, BD, 564279, 748371, FITC, Biolegend 103107), CD45.1 (A20, PE, Biolegend 110707), CD3e (clone 145-2C11, BUV395, BD563565, APC, Biolegend 100312, clone KT3.1.1, BV421, Biolegend 155617), CD4 (clone GK1.5, BV650, BD 563232), CD8a (clone 53-6.7, BV605, BD 563152, APC, Biolegend 100711), CD11c (clone HL3, BUV737, BD612796, clone N418, PE, Biolegend 117307), CD19 (clone 1D3, BB700,BD 566412), CD86 (clone GL1, BUV395, BD 564199), CD80 (clone 16-10A1, PE/Cy5, Biolegend, 104711), CD103 (clone 2E7, BV421, Biolegend, 121421), NK1.1 (clone PK136, PE/Cy5,Biolegend 108715), MHCII (clone M5/114.15.2, BV421, BV711, BV650, Biolegend 107631,107643,107641), CD40 (clone 1C10, PerCP-eFluor710, eBioscience 46-0401-82), CD69 (clone H1.2F3, BUV737,BD 612793, BV421, Biolegend 104527), Ly6G (clone 1A8, BV785, Biolegend 127645), Ly6C (clone HK1.4, AF700, Biolegend 128023). The following anti-human antibodies were used for immunostaining: HLA-DR (clone G46-6, BV480, BD566154), CD11C (clone B-ly6, BV711, BD563130), CD45RA (clone HI100, PE,BD555489), CD25 (clone 2A3, BUV737, BD612807), CD44 (clone G44-26, APC/H7, BD,560532), CD62L (clone DREG-56, BV510, BD563203), CD8 (clone RPA-T8, BUV395, BD563795), CCR7 (clone G043H7, BV785, Biolegend353230), CD3 (clone BW264/56, APC, Miltenyi Biotec 130-113-

687).

For peptide-MHC-dextramer staining, 10µl dextramer (PE-H-2Kb SIINFEKL, or APC-H-2Db Adpgk, Immudex) were added and incubated at room temperature for 15 min. Anti-mouse H-2K^{b} bound to SIINFEKL antibody staining (Clone 25-D1.16, APC, PE/Cy7, Biolegend, 141605) was performed at 37°C for 15 min. Cells were washed and resuspended in 300 µl FACs buffer with viability dye (DAPI, Biolegend, 3 µM; or Propidium Iodide, Invitrogen, 1.7 µg/ml; or DRAQ7, Biolegend, 2 µM) and characterized using an 18-colour BD LSR Fortessa (BD Biosciences) or Beckman Coulter Cytoflex. Acquired data were analyzed using FACSDiva 6 (BD Biosciences) and FlowJo 10 (BD). Cell counts were calculated using Counting Beads (C36950, C36995, ThermoFisher).

When intracellular staining needs to be performed, cells were first stained with viability dye (eBioscience™ Fixable Viability Dye eFluor™ 780, 65-0865-18), followed by surface staining as previous described. For intracellular staining, cells were fixed and permeabilized using Foxp3 / Transcription Factor Staining Buffer Set (eBioscience, 00-5523-00). Upon wash with permeabilization buffer, the intracellular antibody (anti-mouse Foxp3, clone MF-14, AF647, Biolegend, 126408) was added and incubated for 30 min at room temperature.

RNA extraction, reverse transcription and qPCR

Cells were collected at the indicated time points and lysed using Trizol Reagent (Invitrogen). Tissues were homogenized in Trizol (Invitrogen) using a Precellys 24

(Bertin) bead mill homogenizer. Lysed and homogenized samples were processed using a Direct-zol RNA MiniPrep kit (Zymo Research) according to the manufacturer's instructions. RNA quantity and quality was analyzed using a Nanodrop 2000 (ThermoFisher) or Bioanalyzer. Reverse transcription was performed using PrimeScript™ RT Reagent Kit (Takara) according to the provided instructions. Q-PCR analyses were performed using PowerUp SYBR Green (Applied Biosystems): primer sequences are provided in **Supplementary Information Table 4**. Quantification of the transcript was performed using the $2^{-\Delta\Delta Ct}$ method using *Rplp0, Rpl32, and/or Gapdh,* as internal reference genes.

***In vivo* antibody treatments**

To deplete specific leukocyte subsets, depletion antibody or isotype control were injected i.p. 1 day before the tumor inoculation, and repeated every 3 days. The following antibodies were used, anti-mouse CD4, clone GK1.5, 100µg; anti-mouse CD8a, clone YTS 169.4, 100µg; anti-mouse Ly6G, clone 1A8, 200µg, all from BioXCell. For anti-CD80 treatment, 200µg anti-mouse CD80 antibody (clone 16-10A1, BioXCell) or isotype control (BE0091, BioXCell) were given i.p 1 day before the tumor inoculation, and repeated every 3 days.

Human monocyte-derived DCs

Human peripheral blood mononuclear cells (PBMCs) were collected from healthy donors' buffy coat (provided by University Hospitals of Geneva (HUG), Switzerland)

683 using Ficoll-Paque Plus (Cytiva). Monocytes (MoDCs) were isolated using a Classical
684 Monocyte Isolation Kit (human, Miltenyi Biotec) according to the manufacturer's
685 instructions. Cells were spun down and resuspended into complete medium (RPMI, 10%
686 heat-inactivated FCS, 2 mM L-glutamine, 1% penicillin-streptomycin, 50 µM β-
687 mercaptoethanol) plus 500U/mL human GM-CSF and 250U/mL human IL-4 (both
688 from Miltenyi Biotec) and cultured in 12-well cell culture plate at 37°C with 5% CO_2.
689 The medium was refreshed every other day. On day 6, non-adherent cells were collected
690 for experiments.

691

692 **Proliferation Assays**

693 Mouse spleen and lymph nodes were harvested from OT-I mice and then passed through
694 a 70 µm cell strainer. After obtaining single-cell suspension, naïve $CD8^+$ T cells were
695 purified using a cell isolation kit (Miltenyi) according to the manufacturer's instructions.
696 Cells were adjusted to 2×10^6 cells/ml concentration and stained using Cell Trace Violet
697 Proliferation Kit (C34557, Invitrogen) at a final concentration of 5 µM in PBS for 15
698 min at 37°C. LPS-matured BMDCs were loaded with 10nM OVA-peptide SIINFEKL
699 for 15min at 37°C. Then 1,000 BMDCs were co-cultured with 10,000 naïve CD8 T
700 cells in 200µl complete medium (RPMI, 10% heat-inactivated FCS, 2 mM L-glutamine,
701 1% penicillin-streptomycin, 50 µM β-mercaptoethanol, 1mM pyruvate sodium) in a 96-
702 well round bottom plate. Plates were incubated at 37°C with 5% CO_2 for 48h before
703 analysis. For polyclonal proliferation assays, naïve CD8 T cells were collected from
704 C57BL/6N mice and labelled as described above. A total of 1,000 LPS-matured

BMDCs were co-cultured with 10,000 naïve $CD8^+$ T cells in 200µl complete medium (RPMI, 10% heat-inactivated FCS, 2 mM L-glutamine, 1% penicillin-streptomycin, 50 µM β-mercaptoethanol, 1mM pyruvate sodium) supplemented with anti-mouse CD3 antibody (1µg/mL, ThermoFisher, Cat.16-0032-82) to provide the TCR signal. Human MoDCs were synchronized using horse serum as described above. Before co-culture with T cells, hMoDCs were matured with LPS (200ng/mL) for 24h. To assess proliferation, HLA-$A2^+$ MoDCs were used and loaded with Melan-$A_{26\text{-}35(A27L)}$ peptide (ELAGIGILTV ('ELA'), 10µg/mL)) 24h prior to co-culture. For naïve T cell proliferation assays, human $CD8^+$ T cells were isolated from PBMCs (the same donor as hMoDC) using a $CD8^+$ T cell isolation kit (Miltenyi Biotec) then labelled with Cell Trace Violet (Invitrogen™). 10,000 labelled T cells were co-cultured with 1,000 matured hMoDC, together with 5µg/mL anti-human CD3 antibody (Invitrogen™, Catalog # 16-0037-81). Five days later, T cells were collected for flow cytometry analysis. For patients' T cell proliferation assays, antigen-specific $CD8^+$ T cells were FACS sorted from PBMC of melanoma patients using PE-conjugated HLA-A2/ELA multimers. $Multimer^+$ cells were cloned by limiting dilution and expanded with phytohemagglutinin (PHA) and allogenic feeder cells in a medium containing 150 U/ml human recombinant IL-2 (hrIL-2), as previously described [20]. Then, single clones of T cells were used for co-culture with hMoDC in a ratio of 5:1. On day 5, cells were harvested for flow cytometry analysis.

Vaccinations

Unless specified, 30µg OVA together with 20µg CpG OND 1826 and 20 µg Poly(I:C) (VacciGrade, all from InvivoGen) were injected s.c. into tumor-bearing mice adjacent to the tumor. For vaccination with BMDCs, 1 million SIINFEKL loaded LPS-matured BMDCs were injected together with 20µg CpG and 20µg Poly(I:C). Tumor volume was then measured every one or two days using a caliper. The human vaccination trial was performed as previously detailed[20]. The times of vaccination were stratified into vaccinations performed before or after 1pm. Patients included received all their vaccinations before or after this cutoff time.

***In vitro* cell treatment**

SIINFEKL-loaded, LPS-matured BMDCs were adjusted to a concentration of 1 x 10^6 cells/well and incubated with anti-mouse CD80 (50µg/mL, 16-10A1, BioXCell) or isotype control for 15 min at 37°C. Then, proliferation assays were performed as described above.

Immunofluorescence imaging

B16-F10-OVA cells were cultured as mentioned above, and labelled with CellTrace™ Violet (Invitrogen). Cells were counted and resuspended into PBS, then an equal volume of cold Corning® Matrigel® was added and mixed thoroughly with tumor cells. One million cells in 50µl were injected s.c. into the right flank of the mouse. 4h later, matrigels were harvested directly into 4% PFA and stored at +4°C for 4 hours. Matrigels were kept in 30% sucrose (Sigma) overnight at +4°C after fixation, embedded into OCT

749 blocks (CellPath) and kept at -80°C. Matrigels were subsequently dissected and
750 processed for cryosectioning with 50 µm serial cryosections being cut and processed
751 for immunohistochemistry. Sections were postfixed with 4% PFA for 10 min at RT.
752 Following three washes with PBS, they were incubated with blocking buffer (PBS with
753 20% normal goat serum and 0.5% Triton-100X) for 2 hr at RT. After three consecutive
754 washes with PBS, the sections were stained with an antibody mix of FITC conjugated
755 mouse anti-CD45 (Clone: 30-F11; Biolegend), PE/Dazzle594 conjugated mouse anti-
756 CD11b (Clone: M1/70; Biolegend), Alexa Fluor F647 conjugated mouse anti-CD11c
757 (Clone: N418, Biolegend) diluted in the same blocking buffer as before and incubated
758 overnight at +4°C. Sections were washed three times with PBS before mounting in
759 Fluoromount Aqueous Mounting Medium (Sigma). Images of matrigels were obtained
760 as sections using a Zeiss Axio Examiner.Z1 confocal spinning disk microscope
761 equipped with 405-, 488-, 561- and 640-nm laser sources. Step size was determined as
762 4 µm and images were acquired at 20x magnification. All image analyses were
763 performed in ImageJ. Volume fractions were obtained from binary images in a 3D
764 environment by thresholding the voxels for both Matrigel volume and the signals of
765 interest.

766

767 **Sorting of CD11c^{+}MHCII^{+} cells and RNA sequencing**

768 To obtain dendritic cells (DCs), draining inguinal LNs were collected from mice 24h
769 after tumor engraftment and harvested at 4 time points (ZT3, 9, 15, and 21; n = 5 mice
770 for control, n = 3 mice for *Clec9acre:Bmal1^{flox}* and n = 3 mice for sham-injected mice).

771 LNs were digested as previously described, and $CD45^{+}CD11C^{+}MHCII^{high}$ cells were
772 sorted using an Astrios sorter (Beckman). Flow cytometry sorted DCs were collected
773 in RNAprotect Cell Reagent (cat. #76526, Qiagen). RNA was isolated using an RNeasy
774 Plus Micro Kit (cat. #74034, Qiagen) according to the manufacturer's instructions.
775 RNA integrity and quantity were assessed with a Bioanalyzer (Agilent Technologies).
776 cDNA libraries were constructed by the Genomic platform of the University of Geneva
777 as follows: The SMART-Seq v4 kit from Clontech was used for the reverse
778 transcription and cDNA amplification according to the manufacturer's specifications,
779 starting with 1 ng of total RNA as input. 200 pg of cDNA were used for library
780 preparation using the Nextera XT kit from Illumina. Library molarity and quality were
781 assessed with the Qubit and Tapestation using a DNA High sensitivity chip (Agilent
782 Technologies). Libraries were pooled and loaded for clustering on 2 lanes of a Single-
783 read Illumina Flow cell. Reads of 50 bases were generated using the TruSeq SBS
784 chemistry on an Illumina HiSeq 4000 sequencer.

785 Reads were aligned with STAR v.2.7.0[22] to the mouse mm10 UCSC genome.
786 Gene expression was quantified with HTSeq v.0.9.1. Differential expression analysis
787 was performed with the R/Bioconductor edgeR package . The counts were normalized
788 according to the library size and filtered. Genes having a count above 1 count per
789 million reads in at least 5 samples were kept for subsequent analysis. Tests for
790 differentially expressed genes were done with a GLM (general linear model) using a
791 negative binomial distribution. The genes were considered as differentially expressed
792 when the fold change (FC) was at least 2-fold with a 5% false discovery rate (FDR)

Benjamini-Hochberg multiple testing correction. DiscoRhythm[24] R package version 1.10.0 was used to characterize the rhythmicity present in the provided dataset by performing outlier detection, principal component analysis (PCA) and detection of gene-wise oscillation characteristics. Default parameters were used, except when indicated.

PCA was used to extract the strongest recurring patterns in the dataset. Gene expression values were scaled to a standard deviation of one prior to PCA, such that all genes were on an equal scale. The first four PCA scores were used to detect outliers (flagged by their deviation from the mean). A threshold of three units of standard deviations was used. The Cosinor method was used to test the summarized temporal signal for rhythmicity. PC1 and PC2 were kept as they scored above 10% of the variance each (WT: PC1: 18.9%, PC2: 13.6%; *Bmal1*$^{\Delta cDC}$: PC1: 20.6%, PC2: 12.3%; PBS sham injection: PC1: 20.2%, PC2: 11.6%) suggesting that two main phases of oscillation exist in the data (**Supplementary Information Tables 1-3**). Each gene was tested for rhythmicity with a significance value of a P-value < 0.05. Genes with significant rhythmicity were assigned to two sets, depending on their acrophase (the time in a periodic cycle where a temporal pattern is at its maximum value). Genes with a sincoef > 0 corresponded to an acrophase between 0 and 12 h (PC1), while genes with a sincoef < 0 corresponded to an acrophase between 12 and 24 h (PC2). Both oscillating gene lists were tested for pathway enrichment, using Over-Representation Analyses (ORA) in Gene Ontology Biological Process (GOBP) and Reactome pathways, using ClusterProfiler R[25,26] *(23, 24)* package version 4.4.4. Pathways with an enrichment P-

value < 0.05 were reported as significant.

Chromatin Immunoprecipitation and qPCR

A total of 2×10^7 BMDCs were collected and fixed in PBS containing 1% formaldehyde (Thermo Fisher Scientific) for 10 min at room temperature and quenched with 1M glycine in PBS. Cells were then pelleted and sonicated (Diagenode Bioruptor) to obtain fragments of 0.2–0.8 kilobases in size. Immunoprecipitation was performed with anti-BMAL1 (clone D2L7G, Cell Signaling Technology), anti-Histone H3 (Abcam), or control IgG (Cell Signaling Technology). DNA was isolated with MinElute PCR Purification kits (Qiagen). Q-PCR was performed using PowerUp SYBR Green (Applied Biosystems) in a StepOne™ Real-Time PCR System. Occupancy of BMAL1 at the *Cd80* and *Per2* promoters was quantified by qPCR targeting regions identified as containing E-boxes using the SCOPE motif finder and EPFL eukaryotic database. Relative enrichment was determined as the percentage of input.

Statistical analyses

Unless specified, all data were plotted from independent biological replicates. Data was analyzed using Prism 9 (GraphPad). $*P < 0.05$; $**P < 0.01$; $***P < 0.001$; $****P < 0.0001$. Unless specified, Student's *t*-tests are two-tailed. All other statistical information including *t* or F value and degrees of freedom can be found in the source data.

Methods References

21 Lutz, M. B. *et al.* An advanced culture method for generating large quantities of highly pure dendritic cells from mouse bone marrow. *J Immunol Methods* **223**, 77-92, doi:10.1016/s0022-1759(98)00204-x (1999).

22 Dobin, A. *et al.* STAR: ultrafast universal RNA-seq aligner. *Bioinformatics* **29**, 15-21, doi:10.1093/bioinformatics/bts635 (2013).

23 Anders, S., Pyl, P. T. & Huber, W. HTSeq--a Python framework to work with high-throughput sequencing data. *Bioinformatics* **31**, 166-169, doi:10.1093/bioinformatics/btu638 (2015).

24 Carlucci, M. *et al.* DiscoRhythm: an easy-to-use web application and R package for discovering rhythmicity. *Bioinformatics*, doi:10.1093/bioinformatics/btz834 (2019).

25 Wu, T. *et al.* clusterProfiler 4.0: A universal enrichment tool for interpreting omics data. *Innovation (N Y)* **2**, 100141, doi:10.1016/j.xinn.2021.100141 (2021).

26 Yu, G., Wang, L. G., Han, Y. & He, Q. Y. clusterProfiler: an R package for comparing biological themes among gene clusters. *OMICS* **16**, 284-287, doi:10.1089/omi.2011.0118 (2012).

Acknowledgments

We thank Dr. Barbara Schraml and Dr. Reis e Sousa for providing *Cle9acre* mice. We thank Stéphane Jemelin for help with genotyping and Dr. Flore Sinturel for help with ChIP. We also thank the IGE3 Genomics Platform and the flow cytometry core facility of the University of Geneva. We thank Dr. Liqing Cheng for help with transduction and Dr. Sunwang Xu for discussions. This study received support from the European Research Council (ERC CoG 101001233, CIRCADYN (C.S.)), the Swiss National Science Foundation (SNSF, 310030_182417/1 (C.S.) and 310030_185255 (S.H.)), the Swiss Cancer League (KLS-4836-08-2019 (C.S.)), the Geneva Cancer League (2106 (C.S.)), the EU ITN (813284, INTEGRATA (C.S.)) and the Novartis Foundation for medical-biological Research (20A019 (C.S.)). C.W. is the recipient of a fellowship of the Chinese Scholarship Council (CSC). A.N. and I.C. acknowledge the support of the Italian Association for Cancer Research (IG#22098 to A.N. and MFAG#26482 to I.C.). C.J. is supported by a SNSF PRIMA fellowship (PR00P3_179727), the Swiss Cancer League (KFS 5250-02-2021) and the Geneva Cancer League (GCL, 2007). M.C is the recipient of an iGE3 PhD salary award. M.J.P. receives support from the ISREC Foundation, Ludwig Cancer Research, and NIH grants P01-CA240239 and R01-CA218579. R.B. was funded by a Postdoc Mobility fellowship and a Return Grant of the SNSF (P400PM_183852, P5R5PM_203164). Extended Data Figure 9a, b were created with BioRender.

Author contributions

Conceptualization: CW, CS, CJ, MJP, AN, Stéphanie Hugues, DS, OM; Methodology: CW, BK, IC, RB, LI, NF; Investigation: CW, CB, BK, MC, IC, RB, MS, LG, OG, LI, Stephan Holtkamp; Visualization: YL, RP, NF; Supervision: CS

Writing: CW, CB, BK, MJP, CS

Competing interests

M.J.P. has been a consultant for AstraZeneca, Debiopharm, Elstar Therapeutics, ImmuneOncia, KSQ Therapeutics, MaxiVax, Merck, Molecular Partners, Third Rock Ventures, and Tidal; these relationships are unrelated to the current study. The authors declare no competing interests.

Additional information

All correspondence and requests for materials should be addressed to Christoph Scheiermann.

Data availability

All data that support the conclusions of this paper are available at https://doi.org/10.26037/yareta:t47xfgrgyvbi3kkg7lfidvzw2q. Source data are provided with this paper. The sequencing data have been deposited in the NCBI GEO and are accessible through GEO series accession number GSE217381.

Extended Data Figure 1. Time-of-day of engraftment dictates tumor size

(a) Tumor volume of each mouse after engraftment of B16-F10-OVA cells at 6 different times of the day (*Zeitgeber* time (ZT)); n=10 mice per time point from 2 independent experiments. **(b)** Tumor volume after engraftment of E0771 cells at 2 different times of the day, plotted per group (left) and mouse (right); n=5 mice from 2 independent experiments, two-way ANOVA. **(c-d)** Normalized tumor volume, plotted per group (left) and mouse (right) **(c)** and tumor volume on day 20 **(d)**, after engraftment of 4T1 cells at 2 different times of the day; n=12 (ZT9), n=10 (ZT21) mice from 2 independent experiments, two-way ANOVA **(c)** and unpaired Student's *t*-test **(d)**. **(e)** Normalized tumor volume after engraftment of MC-38 cells at 2 different times of the day, plotted per group (left) and mouse (right); n=8 (ZT9), n=6 (ZT21) mice from 2 independent experiments, two-way ANOVA. **(f)** Fluorescence flux in photons/seconds of B16-F10-OVA-Luc (5×10^5 cells) tumors on day 5 after engraftment; n=8 (ZT9), n=7 (ZT21) mice from 2 independent experiments, unpaired Student's *t*-test. **(g)** Tumor volume in phase-shifted mice injected using the same batch of B16-F10 cells (without OVA expression); n=9 (ZT9), n=6 (ZT21) mice from 2 independent experiments, two-way ANOVA. **(h)** Scheme of the normal (light:dark), inverted lighting (dark:light) and jet lag protocols. For the jet lag, every three days mice were placed into a 6h- or 12h-phase delayed environment. The red dots represent the time when tumors were engrafted (9h after the start of the cycle). All data are represented as mean ± SEM, all *t*-tests are two-tailed.

Extended Data Figure 2. Depletion of CD4 T cells and neutrophils

(a) Flow cytometry gating strategy of tumor infiltrating leukocytes. **(b)** Normalized cell numbers of tumor infiltrating leukocytes after 14 days of tumor engraftment; from ZT1 to 21, n=10, 9, 10, 7, 10, 8 mice from 4 independent experiments, Cosinor analysis. Treg, regulatory T cells. **(c-d)** Tumor volume upon anti-CD4 antibody depletion, n=4 (ZT9 anti-CD4), n=5 (ZT21 anti-CD4), n=6 (control) mice **(c)**, or anti Ly6G antibody depletion, n=5 (control), n=6 (anti-Ly6G) mice **(d)**, from 2 independent experiments, two-way ANOVA. **(e-j)** Flow cytometry gating strategies and quantification of neutrophils in blood (**e-h**) or tumor **(i-j)** after anti-Ly6G treatment. Anti-mouse Ly6G antibody was given every 3 days, starting 1 day before the tumor inoculation (d-1). Neutrophil frequency after treatment at days 0 and 1 **(e-f)**, from left to right, n=3, 2, 3 mice, or day 12 **(g-j)**, n=3 (iso), n=5 (anti-Ly6G) mice from 2 independent experiments, unpaired Student's *t*-test. All data are represented as mean ± SEM, ns, not significant, all *t*-tests are two-tailed.

Extended Data Figure 3. Leukocyte populations in skin and dLN

(a) Flow cytometry gating strategy of skin myeloid populations. **(b-c)** Number **(b)** and proportion **(c)** of leukocytes at the tumor engraftment site 4h after B16-F10-OVA engraftment; n=8 mice from 2 independent experiments, unpaired Student's *t*-test. Leu, leukocyte; N, neutrophils; EOS, eosinophil; IM, inflammatory monocytes; NK, natural

killer cells. **(d)** Flow cytometry gating strategy of DC subsets in draining lymph nodes (dLN). **(e-i)** Leukocytes, T cell **(e-f)** and DCs **(g-h)** in the dLN, 24h after tumor engraftment (5×10^5 B16-F10-OVA); n=8 mice, from 2 independent experiments, unpaired Student's *t*-test. **(i)** Gating of anti-mouse H-2K^b bound to SIINFEKL$^+$ DCs in the B16-F10-OVA model. All data are represented as mean ± SEM, all *t*-tests are two-tailed.

Extended Data Figure 4. Time-of-day differences exist in other tumor models

(a-d) DCs and T cell numbers in the dLN, 24h after tumor engraftment of MC-38 cells (n=6 mice) (**a**), 4T1 cells (n=6 mice) (**b**), or E0771-OVA cells, n=7 (ZT9), n=6 (ZT21) mice, (**c-d**), from 2 independent experiments, unpaired Student's *t*-test. (**c**) Gating of anti-mouse H-2K^b bound to SIINFEKL$^+$ DCs in the E0771-OVA model. **(e-g)** T cell numbers in the dLN 72h after tumor engraftment of E0771-OVA cells, n=5 (ZT9), n=7 (ZT21) (**e**), or MC-38 cells, n=6 mice (**f-g**), from 2 independent experiments, unpaired Student's *t*-test. **(f)** Gating of Dextramer H-2D^b/ ASMTNMELM bound to CD8 T cells in the MC-38 model and, (**g**) quantification. All data are represented as mean ± SEM, all *t*-tests are two-tailed.

Extended Data Figure 5. Differences in DCs and CD4 T cells in the dLN

(**a**) DCs numbers in the dLN 24h after sham PBS injection without tumor inoculation, n=7 (ZT9), n=8 (ZT21) mice, from 2 independent experiments, unpaired Student's *t*-test. **(b)** DQ-OVA$^+$ DCs in dLN 24h after inoculation; n=4 mice from 2 independent experiments, unpaired Student's *t*-test. **(c)** EdU staining in CD3$^+$CD4$^+$ T cells in the dLN 48h after B16-F10-OVA cell engraftment; n=3 (ZT9), n=4 (ZT21) mice, representative from 2 independent experiments, unpaired Student's *t*-test. All data are represented as mean ± SEM, all *t*-tests are two-tailed.

Extended Data Figure 6. RNAseq analyses of CD11$^+$ MHCII^{hi} cells in the dLN

(a-d) RNAseq analyses of CD11c$^+$ MHCII^{hi} cells in the dLN 24h after B16-F10-OVA cell engraftment in control mice (n=5 mice) or *Clec9acre:Bmal1^{flox}* mice (n=3 mice), from 2 independent experiments. **(a)** Expression (Counts per million (CPM)) of *Per1* and *Dbp* in CD11c$^+$ MHCII^{hi} cells from control mice, Cosinor analysis. **(b)** Principal Component (PC) analyses of each sample from sequencing of CD11c$^+$ MHCII^{hi} DCs in control mice. **(c)** Significantly enriched pathways from PC1 in control cells with CD28 signaling pathways highlighted in red, shown for control and *Clec9acre:Bmal1^{flox}* CD11c$^+$ MHCII^{hi} cells. The vertical dashed line represents the significant *p* values, hypergeometric test. **(d)** GO Biological Process interactions in the PC2 gene cluster for control cells. All data are represented as mean ± SEM.

Extended Data Figure 7. RNAseq analyses in *Clec9acre:Bmal1^{flox}* mice

(a-c) RNAseq analyses of CD11^{+} MHCII^{hi} cells in the dLN 24h after B16-F10-OVA cell engraftment at ZT3, 9, 15 and ZT21 in *Clec9acre:Bmal1^{flox}* mice (n=3 mice). **(a-b)** Significantly enriched pathways from PC1 (**a**) and PC2 (**b**) in *Clec9acre:Bmal1^{flox}* cells, hypergeometric test. **(c)** GO Biological Process interactions in PC2 gene cluster for *Clec9acre:Bmal1^{flox}* cells.

Extended Data Figure 8. RNAseq analyses in sham conditions

(a-c) RNAseq analyses of CD11c^{+} MHCII^{hi} cells in the dLN 24h after PBS injection (n=3 mice) or after B16-F10-OVA cell (n=5 mice) at ZT3, 9, 15 and ZT21 in WT mice, from 2 independent experiments. **(a)** Pathways found significantly enriched by over-representation analysis in the lists of significantly oscillating genes in PC1 (Reactome database) in WT mice. The same pathways from RNAseq analyses in PBS injection mice were also plotted; n=3 mice per time point. The vertical dashed line represents the significant *P* values, hypergeometric test. **(b-c)** Pathways found significantly enriched by over-representation analysis in the lists of significantly oscillating genes in PC1 and PC2 in PBS injection mice, hypergeometric test.

Extended Data Figure 9. Synchronization experiments of BMDCs

(a-b) Synchronization scheme of BMDCs for qPCR analyses (**a**) and co-culture experiments (**b**). **(c)** *Cd80* mRNA expression after synchronization of immature BMDCs from WT (n=15 mice) and *Bmal1$^{-/-}$* (n=4 mice) mice without LPS maturation, Cosinor analysis. **(d)** qPCR of LPS-matured BMDCs at different times after synchronization; n=9 mice from 2 independent experiments, one-way ANOVA. **(e)** Predicted binding regions of BMAL1 to the *Cd80* gene using Eukaryotic Promoter Database with a cutoff *P*-value of 0.001. **(f)** Chromatin immunoprecipitation (ChIP) of BMAL1 binding the promoter of *Per2* of BMDCs after synchronization; n=3 mice, from 2 independent experiments, two-way ANOVA. All data are represented as mean ± SEM, ns, not significant.

Extended Data Figure 10. Time-of-day differences in vaccination efficacy

(a) Tumor volume after B16-F10-OVA cell engraftment at ZT9 and OVA vaccination at ZT9 (120h after tumor engraftment, n=11) or ZT21 (108h, n=12, or 132h, n=11 mice, after tumor engraftment); from 2 independent experiments, two-way ANOVA. **(b-c)** Numbers of DC subsets **(b)** and T cells **(c)** in the draining LN 24h after OVA vaccination (on day 5 after B16-F10-OVA cell engraftment) in control or *Clec9acre:Bmal1^{flox}* mice, n=5 mice from 2 independent experiments, unpaired Student's *t*-test. **(d)** Tumor volume in WT mice after tumor engraftment (B16-F10-OVA cells 5×10^{5}) at ZT9 or ZT21, with

or without OVA vaccination on day 5 (arrow) at ZT9 or ZT21, n=4 mice, two-way ANOVA. **(e)** Tumor volume after B16-F10-OVA cell engraftment at ZT9 and OVA vaccination on day 5 and 8 (arrows), both at ZT9 or ZT21 (n=6 mice) or unvaccinated controls (n=9 mice), from 2 independent experiments, two-way ANOVA. **(f)** qPCR of human *PER2* expression in human monocyte derived DCs (hMoDC) after synchronization, n=3 patients, Cosinor analysis. All data are represented as mean ± SEM, ns, not significant, all *t*-tests are two-tailed.

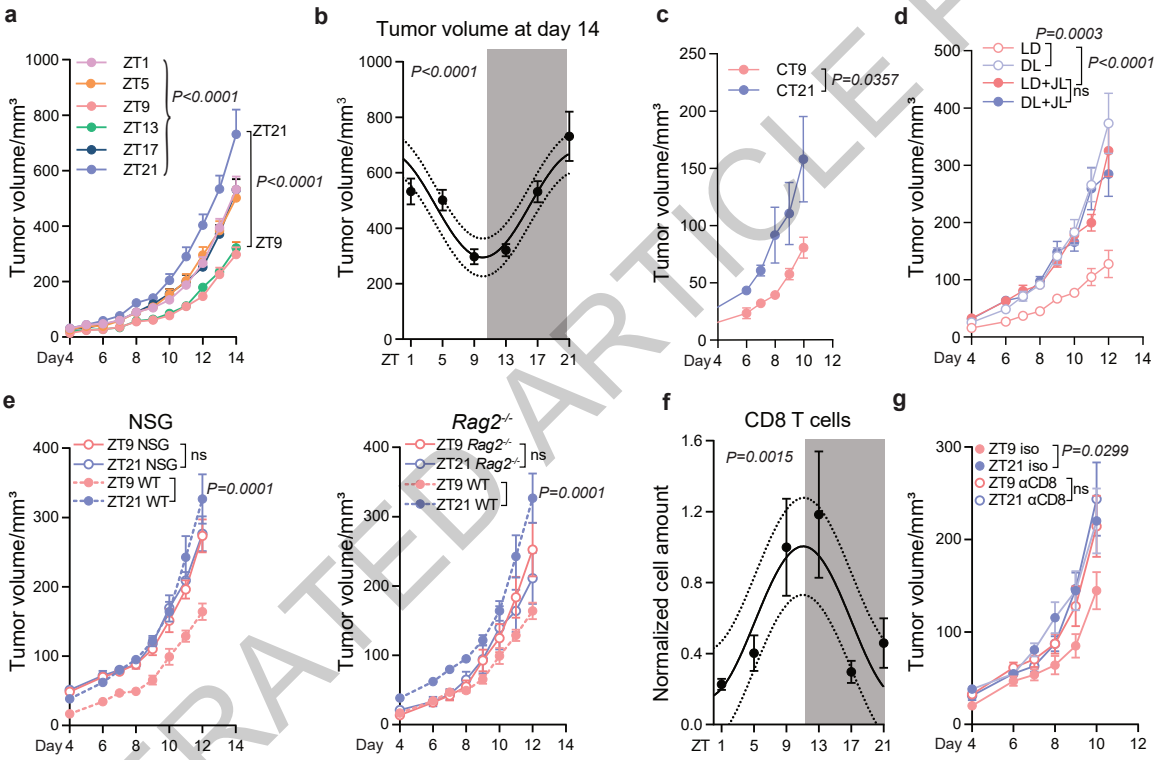

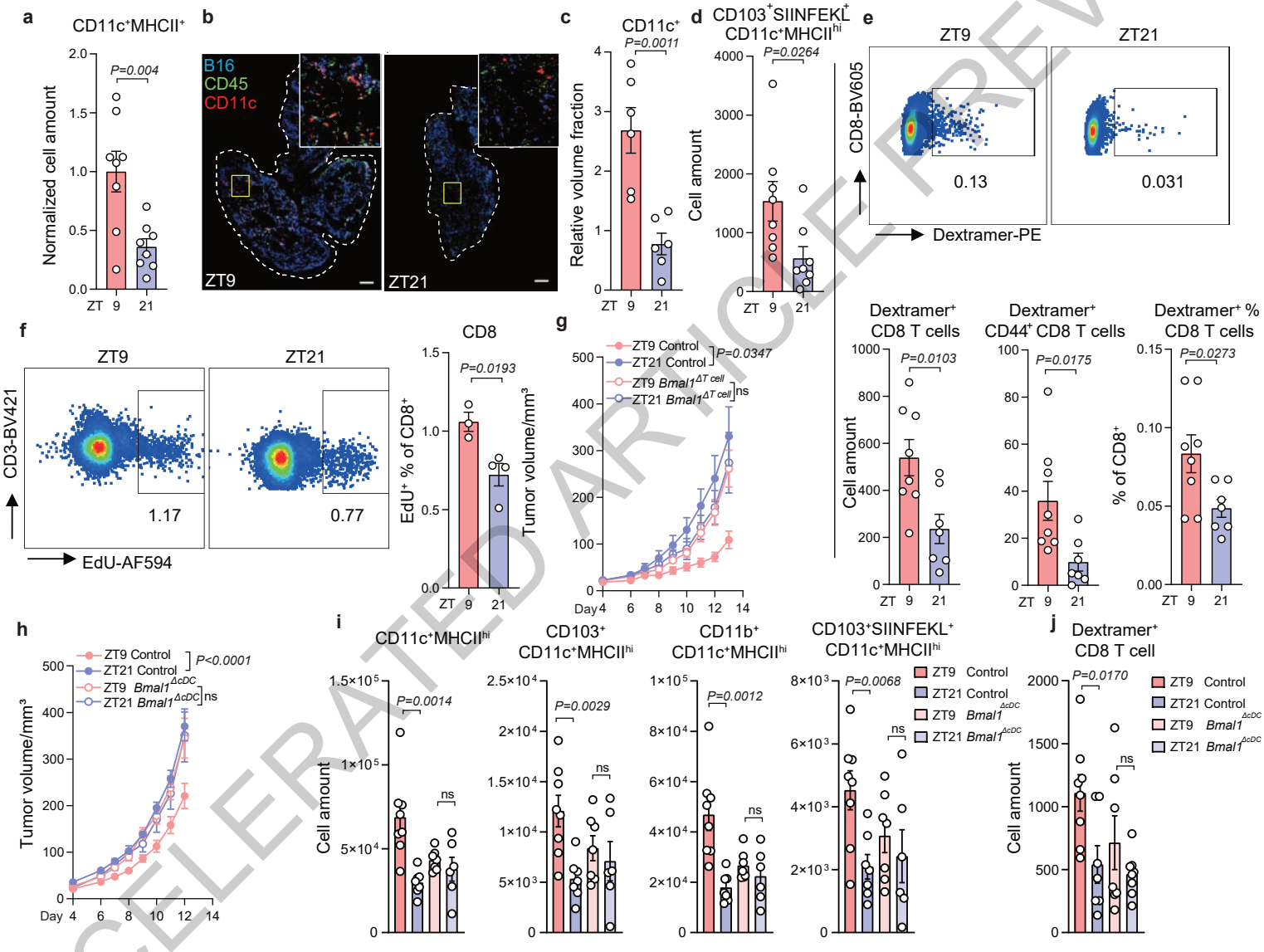

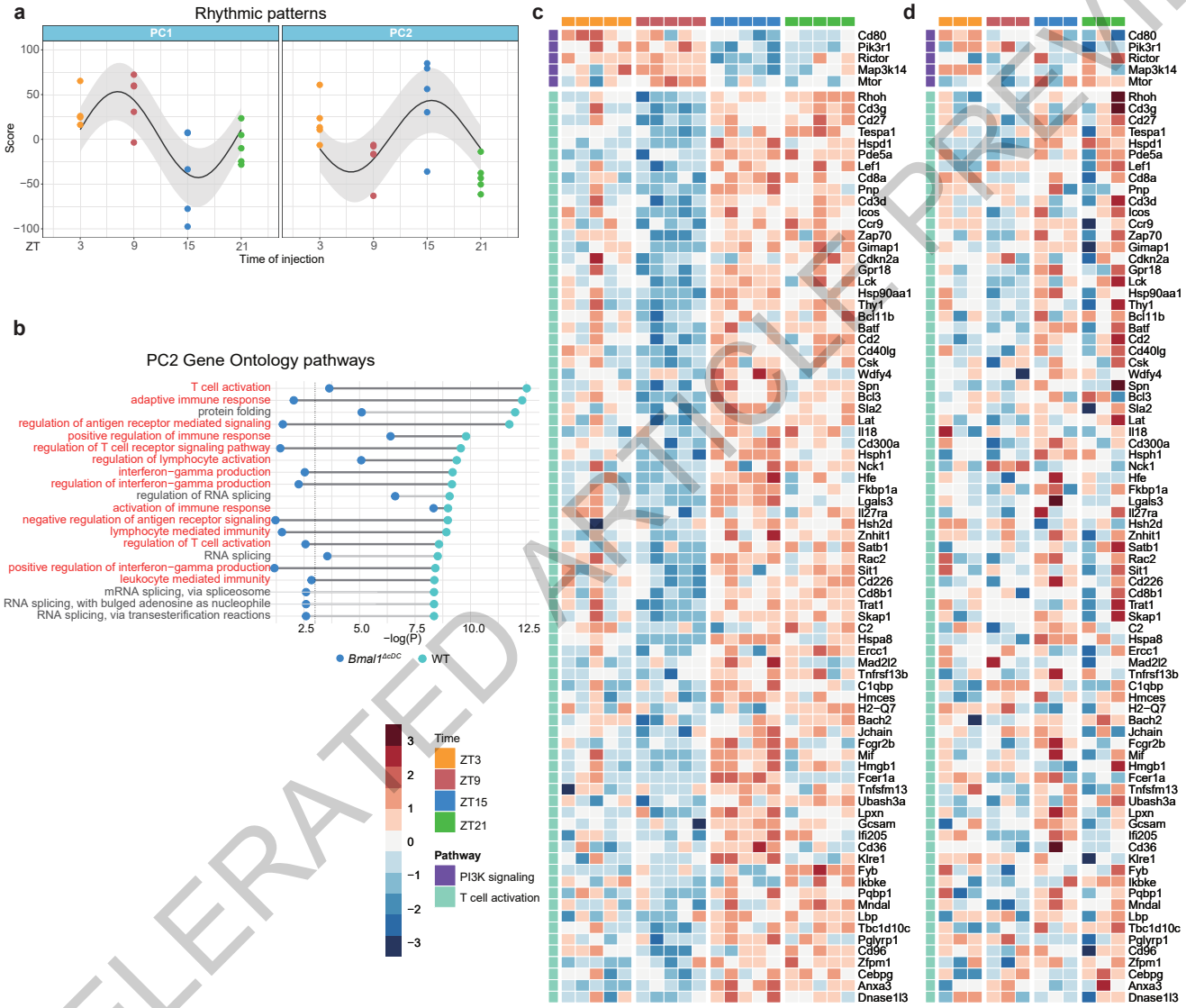

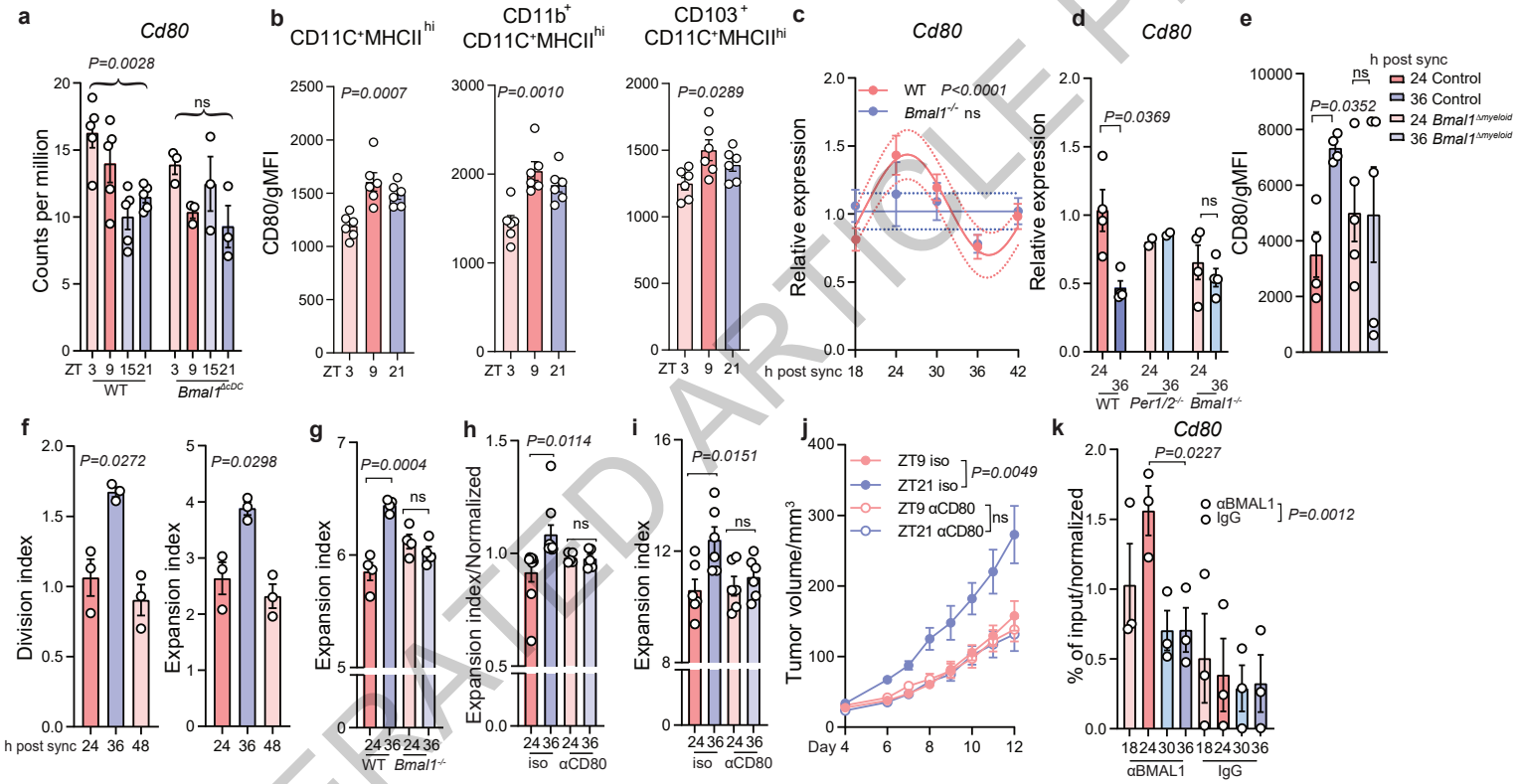

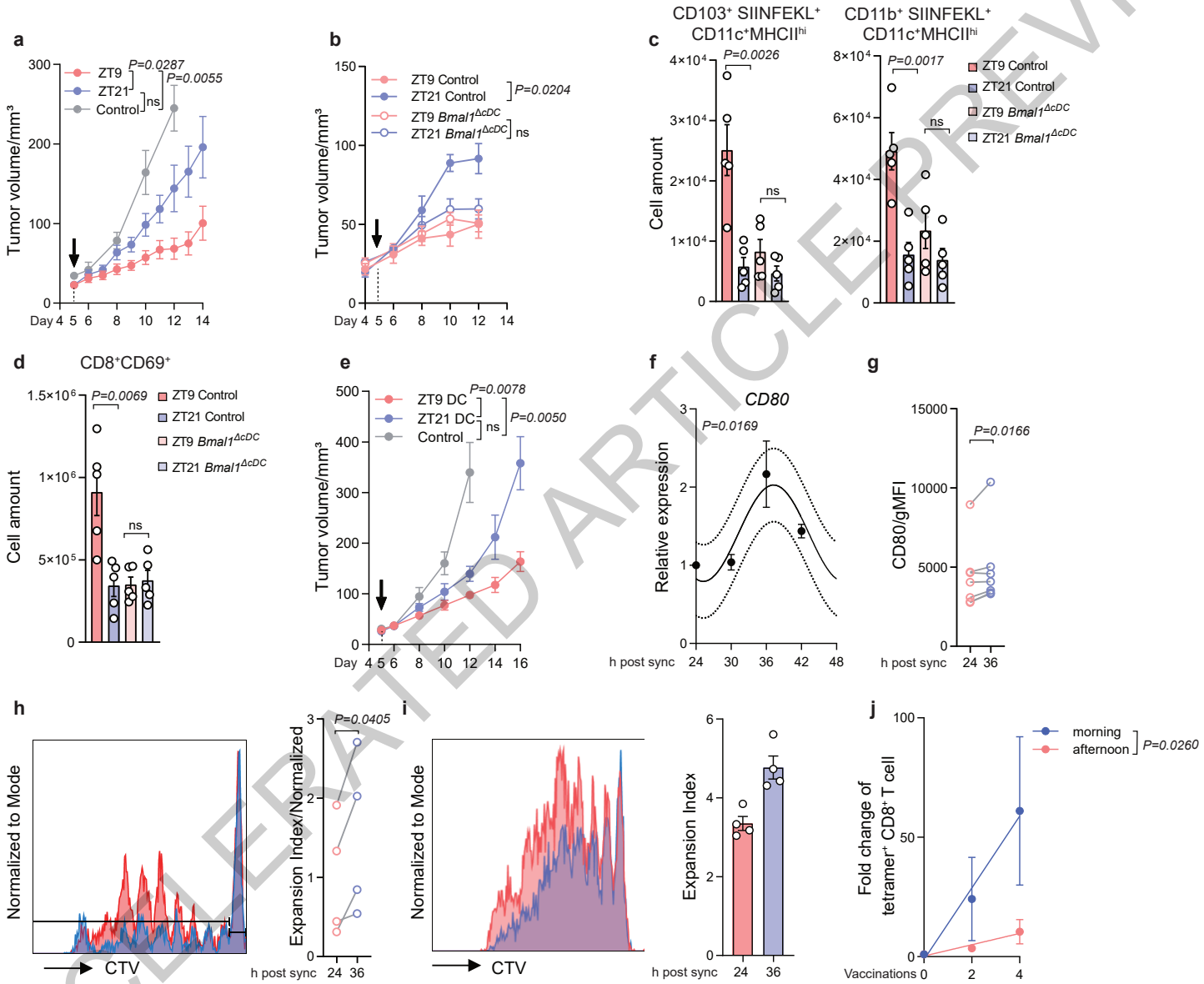

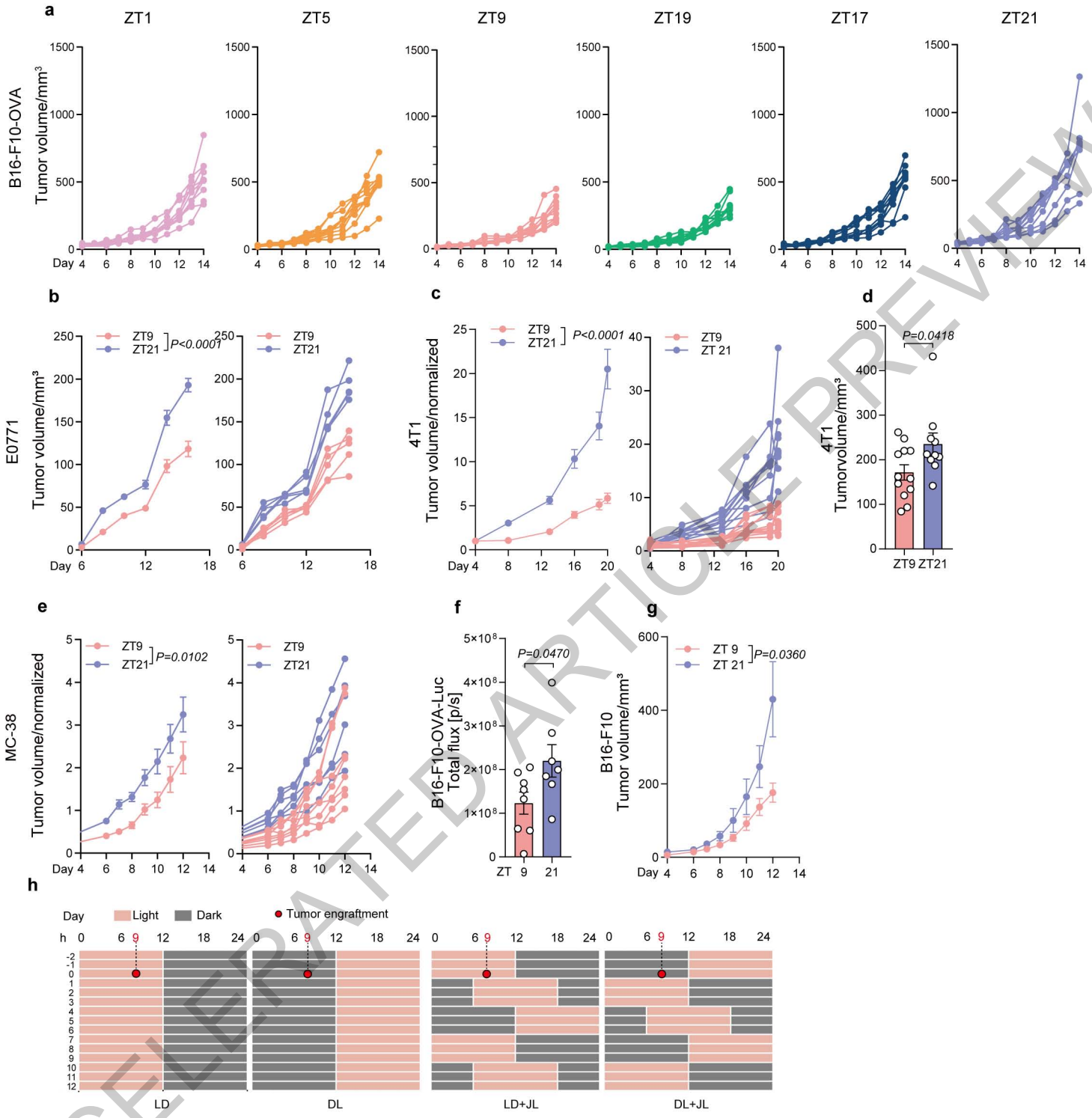

Extended Data Fig. 1

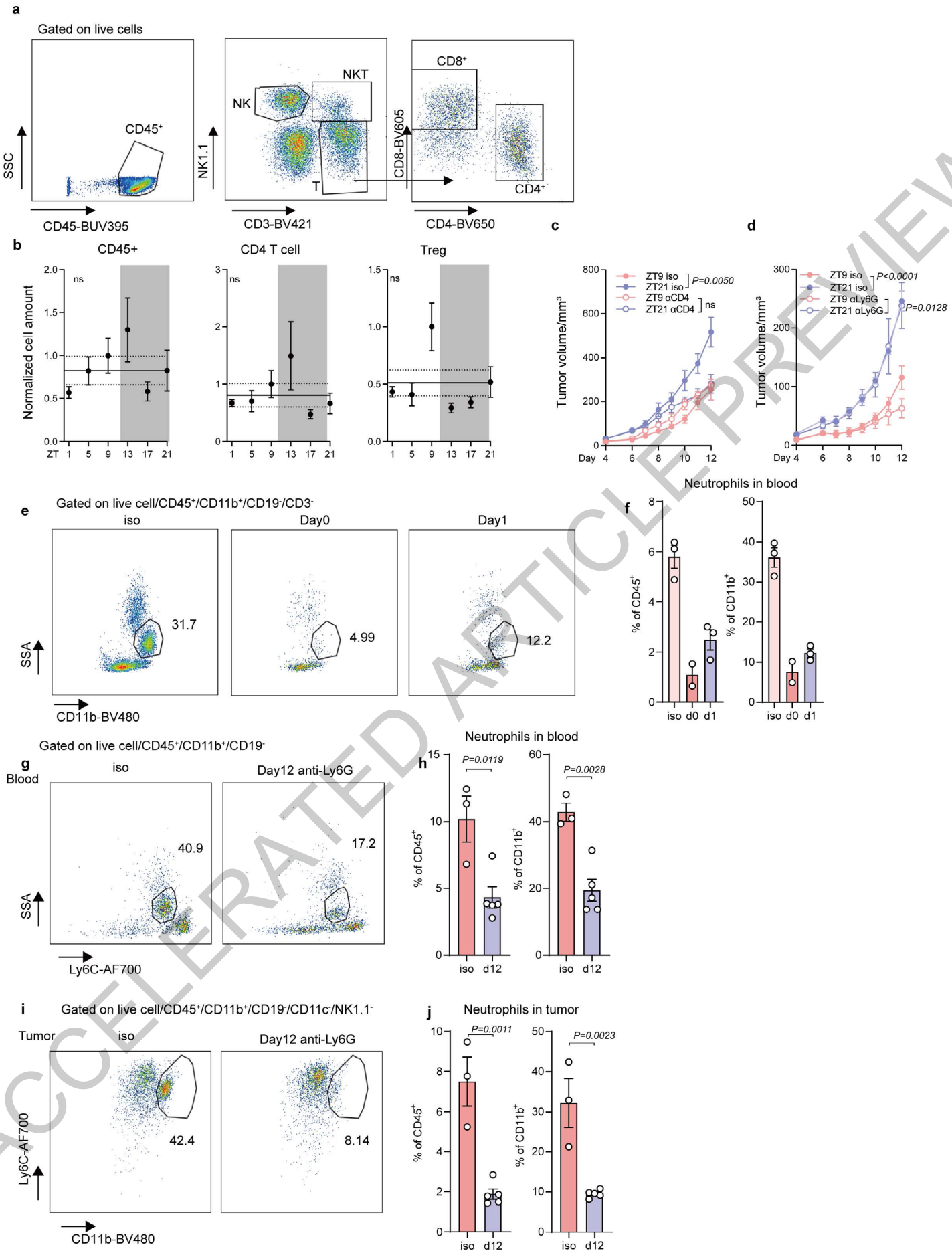

Extended Data Fig. 2

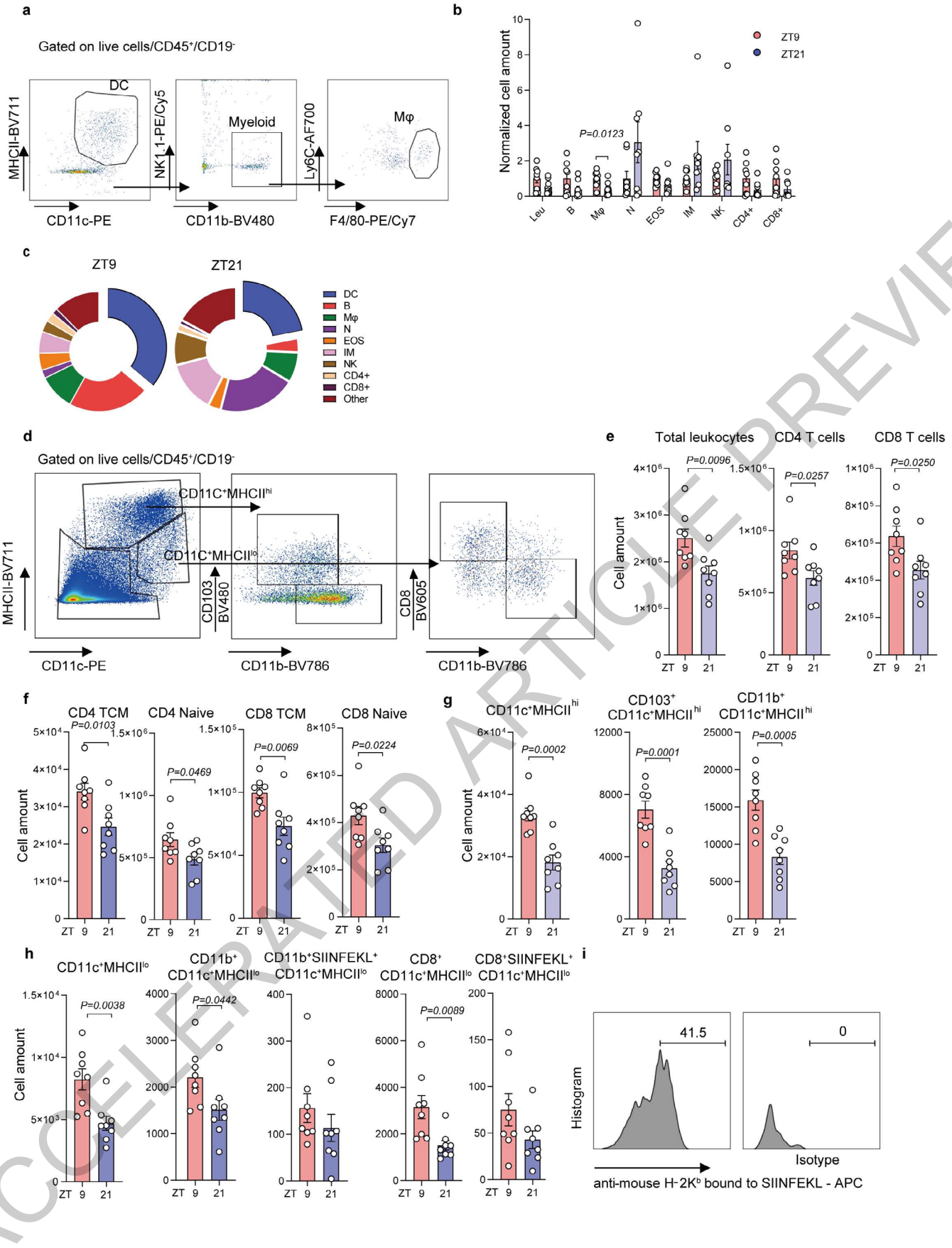

Extended Data Fig. 3

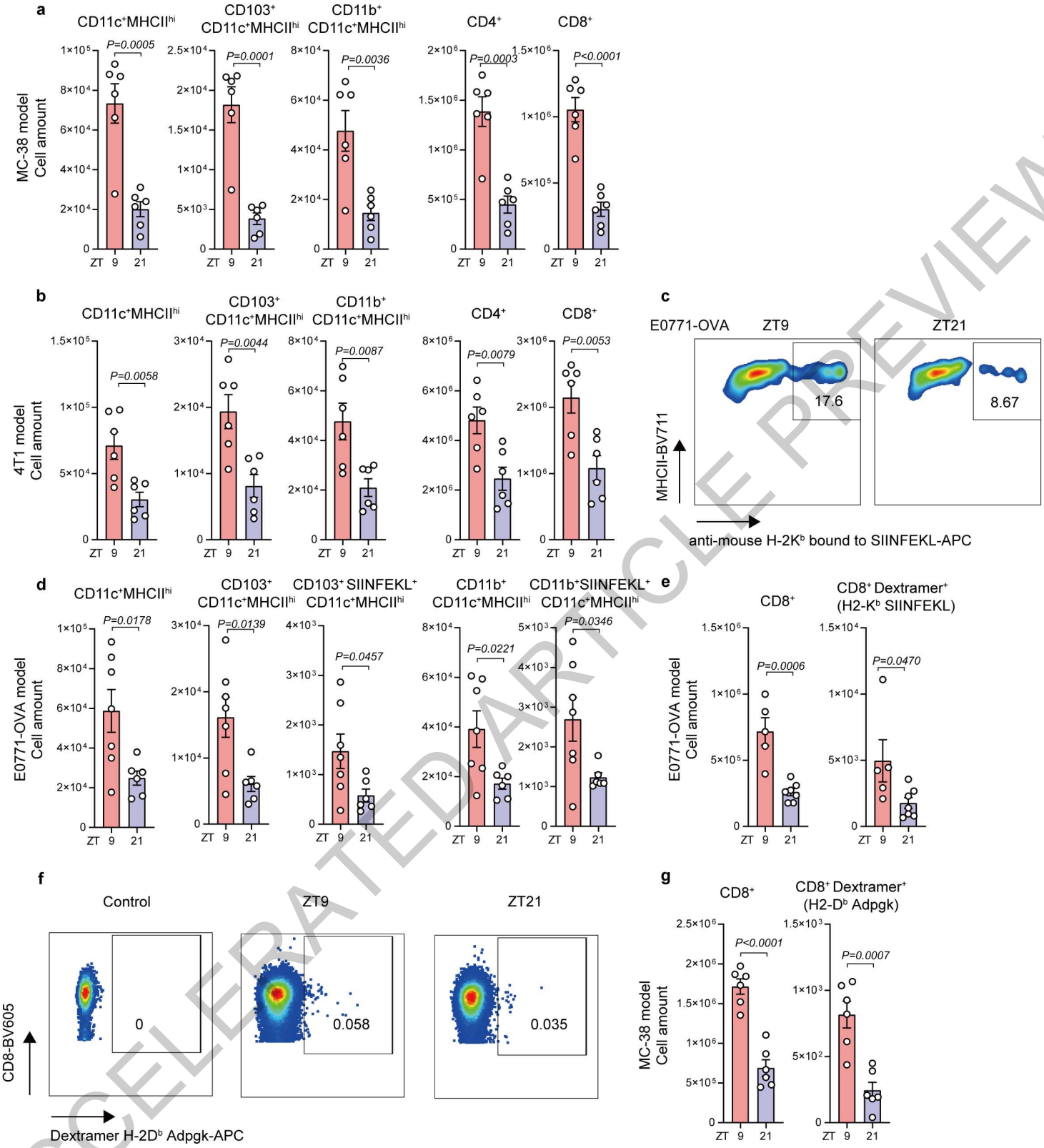

Extended Data Fig. 4

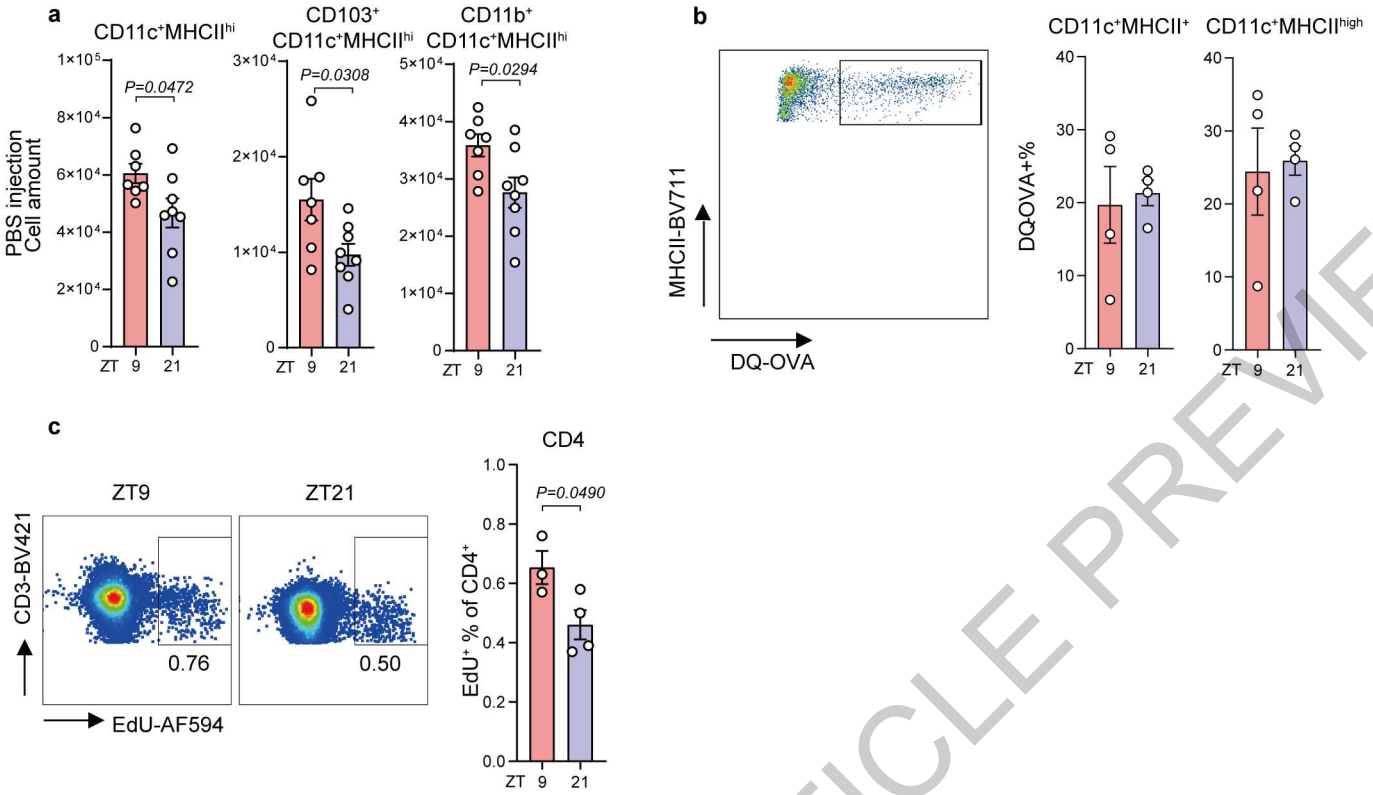

Extended Data Fig. 5

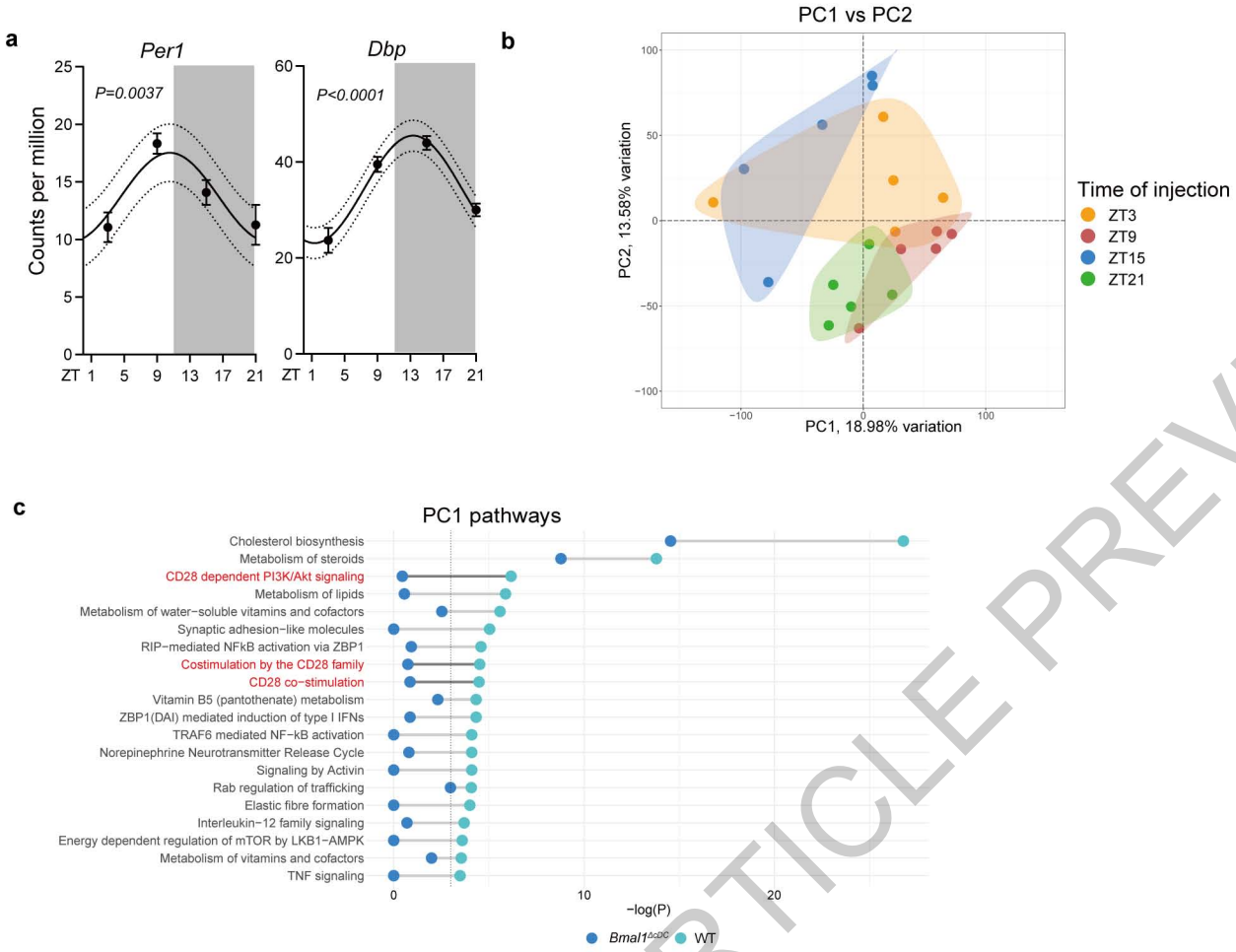

Extended Data Fig. 6

a

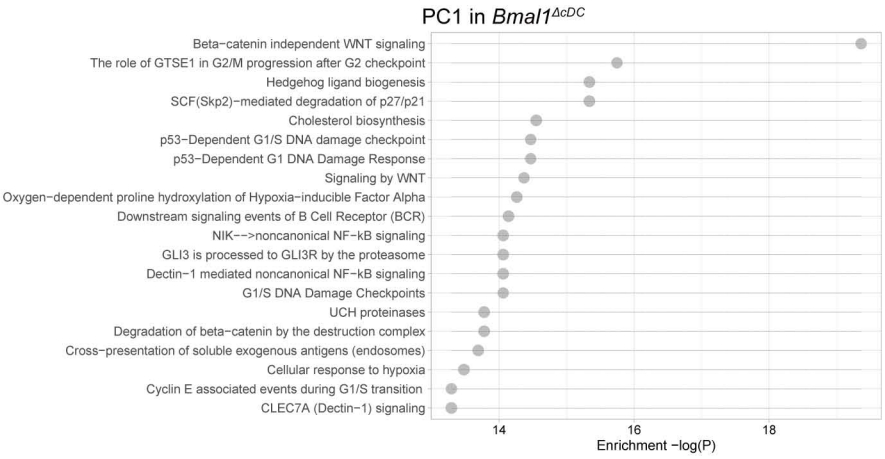

b

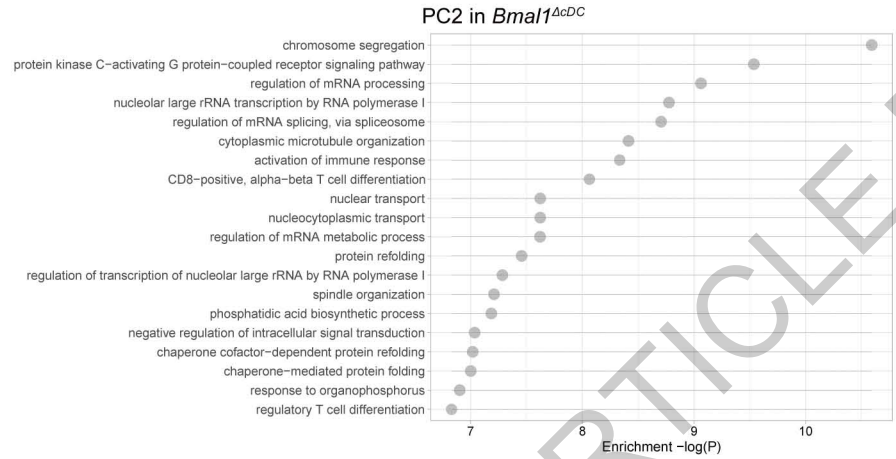

c

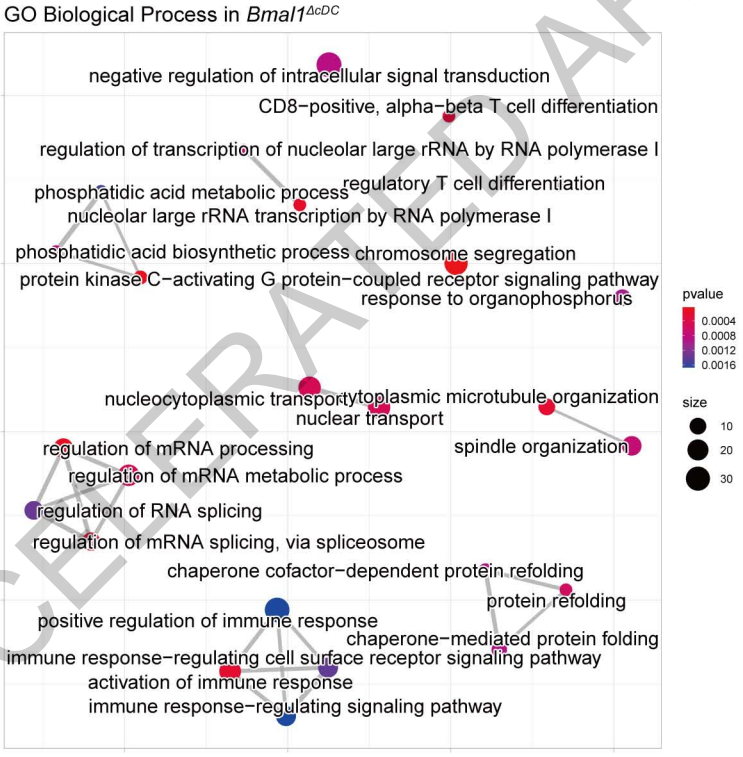

Extended Data Fig. 7

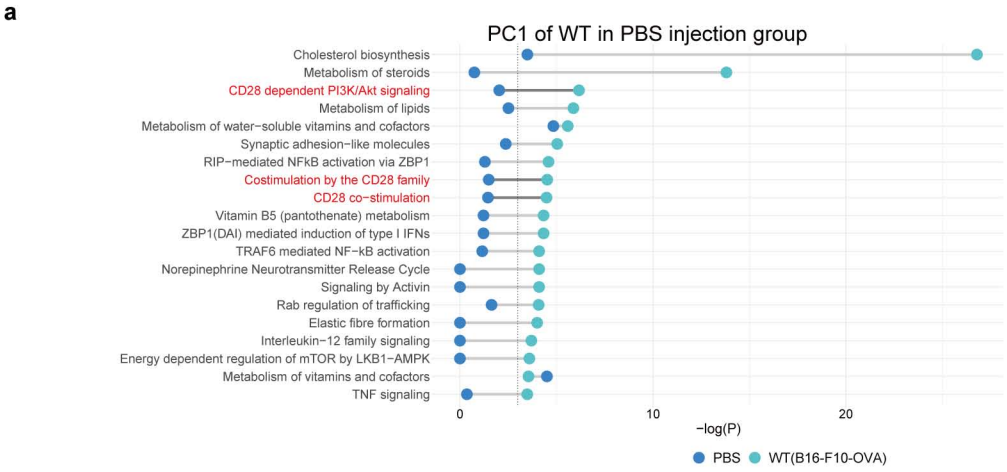

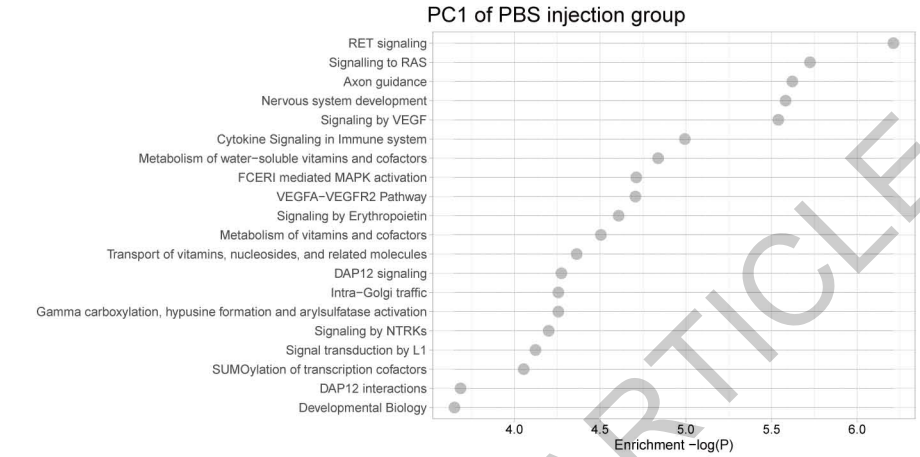

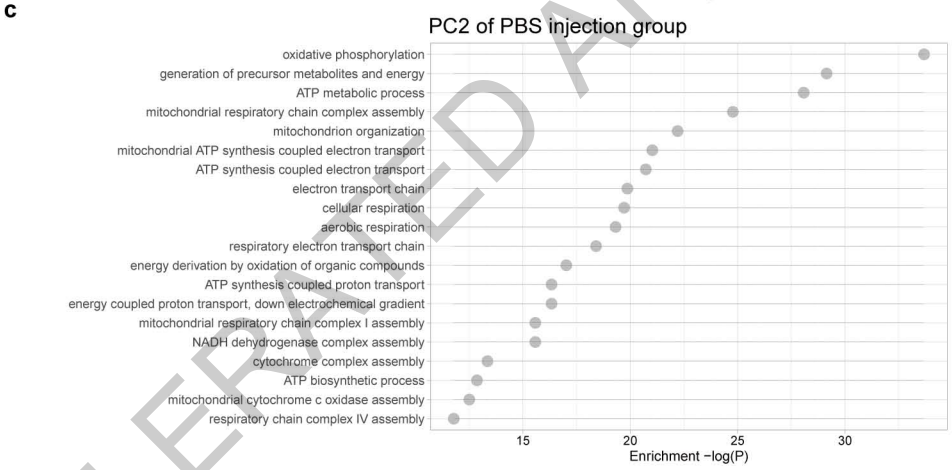

Extended Data Fig. 8

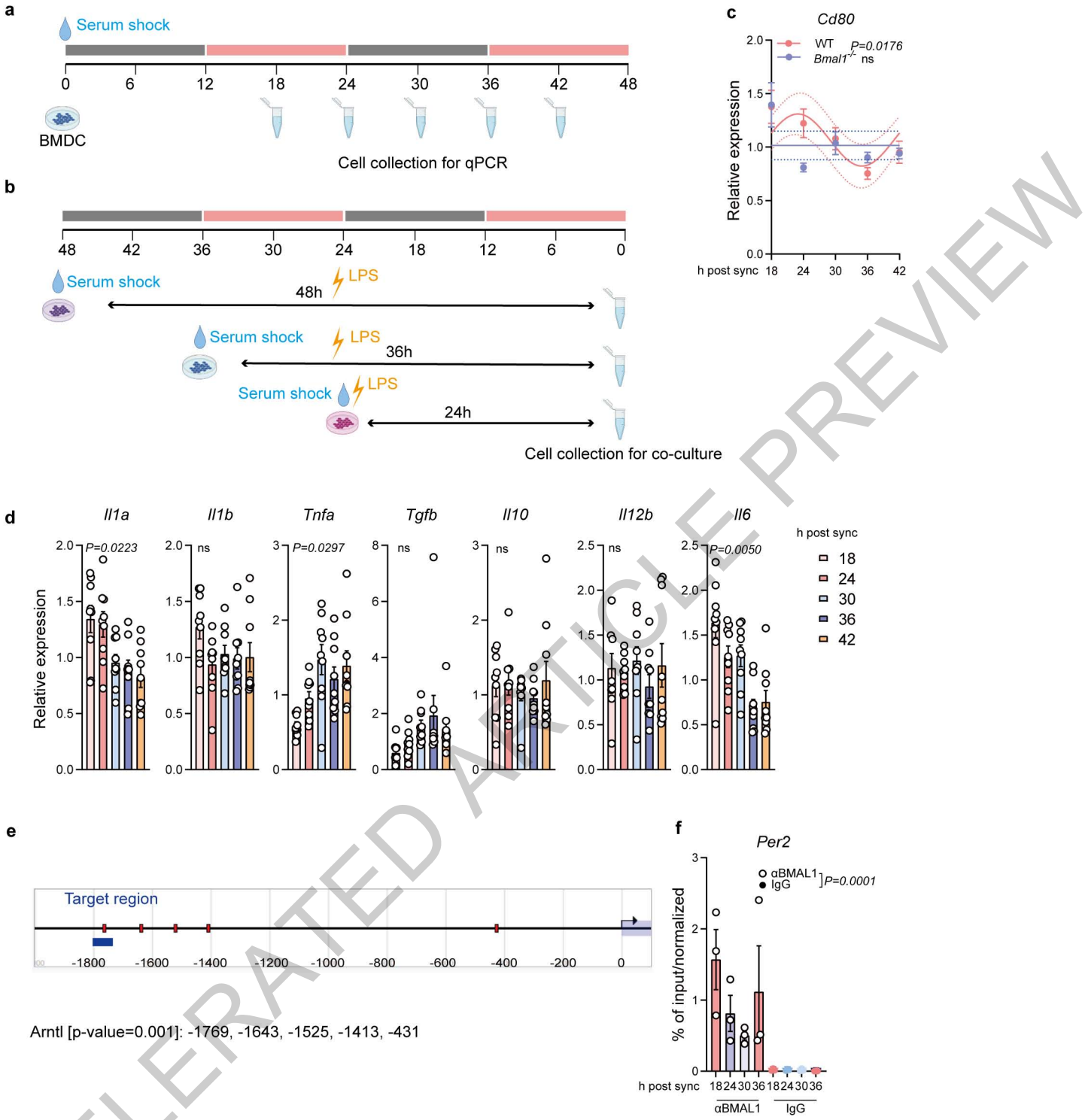

Extended Data Fig. 9

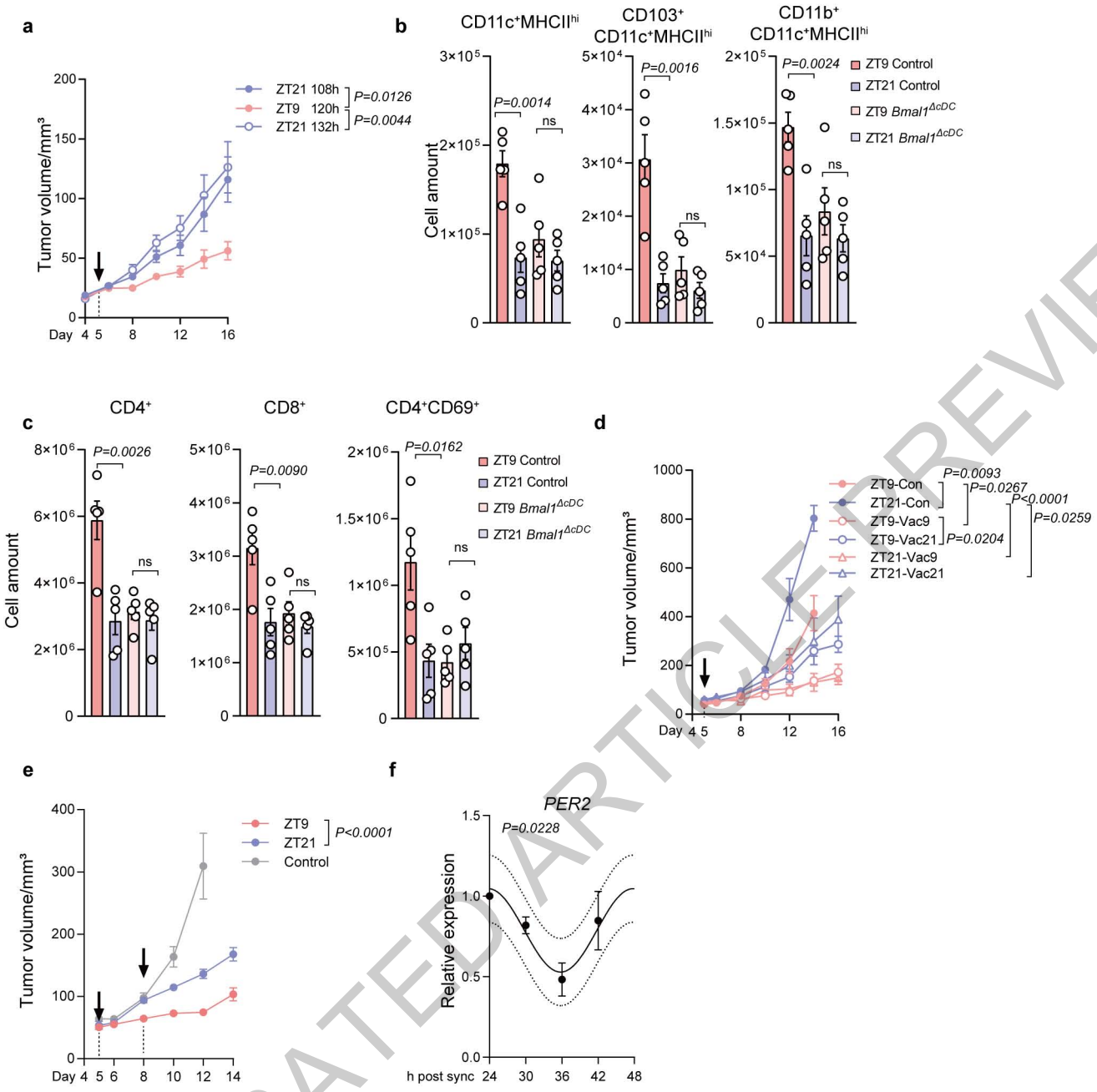

Extended Data Fig. 10

nature portfolio

Corresponding author(s): Christoph Scheiermann

Last updated by author(s): Nov 9, 2022

Reporting Summary

Nature Portfolio wishes to improve the reproducibility of the work that we publish. This form provides structure for consistency and transparency in reporting. For further information on Nature Portfolio policies, see our Editorial Policies and the Editorial Policy Checklist.

Statistics

For all statistical analyses, confirm that the following items are present in the figure legend, table legend, main text, or Methods section.

n/a	Confirmed	
☐	☒	The exact sample size (*n*) for each experimental group/condition, given as a discrete number and unit of measurement
☐	☒	A statement on whether measurements were taken from distinct samples or whether the same sample was measured repeatedly
☐	☒	The statistical test(s) used AND whether they are one- or two-sided *Only common tests should be described solely by name; describe more complex techniques in the Methods section.*
☒	☐	A description of all covariates tested
☐	☒	A description of any assumptions or corrections, such as tests of normality and adjustment for multiple comparisons
☐	☒	A full description of the statistical parameters including central tendency (e.g. means) or other basic estimates (e.g. regression coefficient) AND variation (e.g. standard deviation) or associated estimates of uncertainty (e.g. confidence intervals)
☐	☒	For null hypothesis testing, the test statistic (e.g. *F*, *t*, *r*) with confidence intervals, effect sizes, degrees of freedom and *P* value noted *Give P values as exact values whenever suitable.*
☒	☐	For Bayesian analysis, information on the choice of priors and Markov chain Monte Carlo settings
☐	☒	For hierarchical and complex designs, identification of the appropriate level for tests and full reporting of outcomes
☒	☐	Estimates of effect sizes (e.g. Cohen's *d*, Pearson's *r*), indicating how they were calculated

Our web collection on statistics for biologists contains articles on many of the points above.

Software and code

Policy information about availability of computer code

Data collection	BD FACSDiva, StepOne, SlideBook, Leica Application Suite, Beckman Coulter Cytoflex
Data analysis	Graph Pad Prism v9, ImageJ, FlowJo vl0, R (Discorhythm, R/Bioconductor edgeR, ClusterProfiler V4.4.4, package), Microsoft Excel

For manuscripts utilizing custom algorithms or software that are central to the research but not yet described in published literature, software must be made available to editors and reviewers. We strongly encourage code deposition in a community repository (e.g. GitHub). See the Nature Portfolio guidelines for submitting code & software for further information.

Data

Policy information about availability of data

All manuscripts must include a data availability statement. This statement should provide the following information, where applicable:

- Accession codes, unique identifiers, or web links for publicly available datasets
- A description of any restrictions on data availability
- For clinical datasets or third party data, please ensure that the statement adheres to our policy

Bulk sequencing data are available at GSE. All data that support the conclusions of this paper can be found in resource or from the authors on request.

Field-specific reporting

Please select the one below that is the best fit for your research. If you are not sure, read the appropriate sections before making your selection.

☒ Life sciences ☐ Behavioural & social sciences ☐ Ecological, evolutionary & environmental sciences

For a reference copy of the document with all sections, see nature.com/documents/nr-reporting-summary-flat.pdf

Life sciences study design

All studies must disclose on these points even when the disclosure is negative.

Sample size	For initial experimental design, power analyses were performed to determine sample size.
Data exclusions	Data was not excluded, unless suggested via statistical testing (GraphPad, Identitication of outliers, ROUT method, Q=1%).
Replication	All experiments were replicated at least once to prove reproducibility and only included if obtained results were the same.
Randomization	Mice were randomly allocated into different experimental groups. With respect to human data, due to the retrospective analysis, no randomization was performed.
Blinding	Investigators were blind to genotype and/or treatment where applicable.

Reporting for specific materials, systems and methods

We require information from authors about some types of materials, experimental systems and methods used in many studies. Here, indicate whether each material, system or method listed is relevant to your study. If you are not sure if a list item applies to your research, read the appropriate section before selecting a response.

Materials & experimental systems

n/a	Involved in the study
☐	☒ Antibodies
☒	☐ Eukaryotic cell lines
☒	☐ Palaeontology and archaeology
☐	☒ Animals and other organisms
☐	☒ Human research participants
☒	☐ Clinical data
☒	☐ Dual use research of concern

Methods

n/a	Involved in the study
☒	☐ ChIP-seq
☐	☒ Flow cytometry
☒	☐ MRI-based neuroimaging

Antibodies

Antibodies used

The following anti-mouse antibodies were used for immunostaining: CD45 (clone 30-F11, BUV 395, BUV 737, BD,564279,748371, FITC, Biolegend 103107), CD45.1 (A20, PE, Biolegend,110707), CD3e (clone 145-2C11, BUV395,BD563565, APC, Biolegend100312 , clone KT3.1.1, BV421, Biolegend 155617), CD4 (clone GK1.5, BV650, BD 563232), CD8a (clone 53-6.7, BV605, BD 563152, APC, Biolegend 100711), CD11c (clone HL3, BUV737, BD612796, clone N418, PE,Biolegend 117307), CD19 (clone 1D3, BB700,BD 566412), CD86 (clone GL1, BUV395, BD 564199), CD80 (clone 16-10A1, PE/Cy5, Biolegend, 104711), CD103 (clone 2E7, BV421, Biolegend, 121421), NK1.1 (clone PK136, PE/Cy5,Biolegend 108715), MHCII (clone M5/114.15.2, BV421, BV711, BV650,Biolegend 107631,107643,107641), CD40 (clone 1C10, PerCP-eFluor710,eBioscience 46-0401-82), CD69 (clone H1.2F3, BUV737,BD 612793, BV421, Biolegend 104527), Ly6G (clone 1A8, BV785, Biolegend 127645), Ly6C (clone HK1.4, AF700, Biolegend 128023), anti-mouse H-2Kb bound to SIINFEKL antibody (Clone 25-D1.16, APC, PE/Cy7, Biolegend, 141605, 127645), anti-mouse Foxp3 (clone MF-14, AF647,Biolegend 126408).
The following anti-human antibodies were used for immunostaining: HLA-DR (clone G46-6, BV480, BD566154), CD11C (clone B-ly6, BV711, BD563130), CD45RA (clone HI100, PE,BD555489), CD25 (clone 2A3, BUV737, BD612807), CD44 (clone G44-26, APC/H7, BD,560532), CD62L (clone DREG-56, BV510, BD563203), CD8 (clone RPA-T8, BUV395, BD563795), CCR7 (clone G043H7, BV785, Biolegend353230), CD3 (clone BW264/56, APC, Miltenyi Biotec 130-113-687).
For in vivo treatment, anti-mouse CD4, clone GK1.5, 100µg,BE0003-1; anti-mouse CD8a, clone YTS 169.4, 100µg,BE0117; anti-mouse Ly6G, clone 1A8, 200µg, BE0075, all from BioXCell. For anti-CD80 treatment, 200µg anti-mouse CD80 antibody (clone 16-10A1, BioXCell, BE0024) or isotype control (BE0091, BioXCell) were given.
For ChIP, anti-BMAL1 (D2L7G) Rabbit mAb #14020 CST were used.

Validation

Primary antibodies have been validated by the manufacturer for the specific species. All neutralization antibodies used were taken from publications that have validated the antibodies prior to this study.

Animals and other organisms

Policy information about studies involving animals; ARRIVE guidelines recommended for reporting animal research

Laboratory animals	C57BL/6N and NSG mice were purchased from Charles River, BALB/c mice were purchased from Envigo. Rag2-/- mice (gift from Walter Reith, University of Geneva, Switzerland) were bred at Charles River. Other transgenic mouse lines were bred at ENVIGO: Bmal1flox/flox, Cd4cre (both purchased from Jackson Labs) and Clec9acre (gift from Barbara Schraml, LMU Munich, Germany). Transgenic mice were maintained as homozygous for Bmal1flox/flox and heterozygous for the relevant Cre. CD45.1 OTI (gift from Walter Reith) mice and Bmal1-/- (gift from Charna Dibner, University of Geneva, Switzerland) mice were bred in house. All mice used were females at 6-12 weeks of age.
Wild animals	The study did not involve wild animals.
Field-collected samples	This study did not involve field samples.
Ethics oversight	All animal procedures and experiments were approved and performed in accordance with the guidelines of the animal research committee of Geneva, Switzerland, or by the Italian Istituto Superiore di Sanità (ISS).

Note that full information on the approval of the study protocol must also be provided in the manuscript.

Human research participants

Policy information about studies involving human research participants

Population characteristics	A thorough explanation of all human data is provided in the methods section. PBMCs were from healthy donor`s buffy coat. Antigen specific T cells were from patients with melanoma. More details of the patients` characteristics can be found in Speiser et al JCI 2005.
Recruitment	Human buffy coats were collected from blood donors at the University Hospitals of Geneva. Human vaccination data was a retrospectively analysis of a previous publication (Speiser et al JCI 2005). Due to a retrospectively analysis, no additional recruitment was performed. Patients were divided into "morning" or "afternoon" based on the time they received the vaccines.
Ethics oversight	Written informed consent was obtained for buffy coats from the healthy donors by the University Hospitals of Geneva. The sampling was conducted according to the Declaration of Helsinki and approved by the Commission Cantonale d'Ethique de la Recherche of the University Hospitals of Geneva.

Note that full information on the approval of the study protocol must also be provided in the manuscript.

Flow Cytometry

Plots

Confirm that:

☒ The axis labels state the marker and fluorochrome used (e.g. CD4-FITC).

☒ The axis scales are clearly visible. Include numbers along axes only for bottom left plot of group (a 'group' is an analysis of identical markers).

☒ All plots are contour plots with outliers or pseudocolor plots.

☒ A numerical value for number of cells or percentage (with statistics) is provided.

Methodology

Sample preparation	Single-cell suspensions were prepared and incubated with mouse or human Fc receptor block (anti-mouse CD16/32 Biolegend, human FcR blocking reagent, Miltenyi Biotec) for 10 minutes at room temperature (RT). After incubation, unless specified otherwise, the antibody mix was added directly into the cell suspension and incubated for 15 min at 4°C. For peptide-MHC-dextramer staining, 10µl dextramer (PE-H-2Kb SIINFEKL, or APC-H-2Db Adpgk, Immudex) were added and incubated at room temperature for 15 min. Anti-mouse H-2Kb bound to SIINFEKL antibody staining (Clone 25-D1.16, APC, PE/Cy7) was performed at 37°C for 15 min. Cells were washed and resuspended in 300 µl FACs buffer with viability dye (DAPI, Biolegend, 3 µM; or Propidium Iodide, Invitrogen, 1.7 µg/ml; or DRAQ7, Biolegend, 2 µM) and characterized using an 18-colour BD LSR Fortessa (BD Biosciences). Acquired data were analyzed using FACSDiva 6 (BD Biosciences) and FlowJo 10 (BD). Cell counts were calculated using Counting Beads (C36950, C36995, ThermoFisher). For intracellular staining, cells were fixed and permeabilized using Foxp3 / Transcription Factor Staining Buffer Set (eBioscience, 00-5523-00). Upon wash with permeabilization buffer, the intracellular antibody (anti-mouse Foxp3, clone MF-14, AF647) was added and incubated for 30 min at room temperature. With respect to FACS, LNs were digested and CD45+CD11C+MHCIIhigh cells were sorted using an Astrios sorter (Beckman).
Instrument	18-colour BD LSR Fortessa (BD Biosciences), Astrios sorter (Beckman).
Software	FACSDiva 6 (BD Biosciences) and FlowJo 10 (BD).

Cell population abundance	Post-sort purity was checked after sorting.
Gating strategy	After removal of debris, cells were gated by live cells (negative for DAPI or DRAQ7, or PI) and single cells

☒ Tick this box to confirm that a figure exemplifying the gating strategy is provided in the Supplementary Information.